EasyChair Preprint

№ 9454

Aerothrmodynamic Analysis of Inlet Air Temperature Changes Effects on Aero Engines Performance and Aero Engines Optimization for High Speeds and High Altitudes Flight Conditions

Mohamadreza Sabzehali and Mahdi Alibeigi

August 16, 2023

AEROTHRMODYNAMIC ANALYSIS OF INLET AIR TEMPERATURE CHANGES EFFECTS ON AERO ENGINES PERFORMANCE AND AERO ENGINES OPTIMIZATION FOR HIGH SPEEDS AND HIGH ALTITDUES FLIGHTCONDITIONS

M.Sabzehali, M. Alibeigi

Abstract

In this study, the effects of variations in inlet air temperature, Mach number, and flight altitude on the performance of the Ramjet XRJ47-W-5 turbofan engines, the F135PW100 and EJ200 turbofan engines, and the J85 GE17 turbojet engine have been investigated. Thrust, specific fuel consumption (TSFC), fuel flow rate, thermal and propulsive efficiencies, nitrous oxide emissions (EI NOx), and actual inlet air mass flow rate to the engines have been considered as performance parameters. At a flight altitude of 10000 meters and a Mach number of 0.8, with a 20-degree reduction in inlet air temperature compared to the ISA Standard Atmosphere (International Standard Atmosphere), the F135PW100 and EJ200 turbofan engines, as well as the J85 GE17 turbojet engine, experienced thrust increases of 7.5%, 5.33%, and 11% respectively, and TSFC reductions of 1.21%, 0.96%, and 0.23% respectively. For the Ramjet XRJ47-W-5, at a flight altitude of 10000 meters and a Mach number of 3, with a 20-degree reduction in inlet air temperature compared to ISA, thrust increased by 9.11% and TSFC decreased by 1.62%. With an increase in the Mach number, the impact of inlet air temperature variations on engine performance parameters becomes more pronounced. Using a genetic algorithm, the optimization of the studied engines has been conducted within the flight altitude range of 20000 to 40000 meters and Mach number range of 2 to 4.5, based on maximizing TSF, minimizing TSFC, and maximizing thermal efficiency. Among the optimal cases, considering energy consumption and power approach, the TOPSIS decision-making method has been employed to select the best configuration.

Keywords: F135PW100, RAMJET, OPTIMIZATION, HIGHT ALTITUDE, SUPERSONIC

1. INTRODUCTION

Gas turbine engines are a type of power generation cycle. A gas turbine engine is an internal combustion engine of the rotary machine type. These engines operate based on the Brayton cycle. Gas turbine engines find wide applications in various industries, from oil and gas to petrochemicals, as well as in electricity-generating power plants and aircraft propulsion systems. The simplest configuration of aircraft gas turbine engines is the turbojet engine. In a turbojet, air is initially drawn into the compressor, where it is compressed and pressurized. The compressed air then enters the combustion chamber, where, upon reaction with fuel, its temperature and entropy increase. The resulting high-energy gases are directed into the turbine, where their temperature and pressure decrease. The turbine provides the mechanical power required to drive the compressor. The gases resulting from the combustion of fuel and air exit the turbine and enter the nozzle, where they expand, increasing their velocity before being discharged into the environment. The reaction due to the discharge of the turbine's exhaust gases generates thrust proportional to the velocity and pressure of the flow at the nozzle exit and the ambient pressure [1]. Another type of configuration for aircraft gas turbine engines is the turbofan engine. The major difference between a turbofan engine and a turbojet engine lies in the presence of a core bypass fan located upstream of the compressor. Turbofan engines are classified into two main flows: the bypass flow and the core flow. The primary components of a turbofan engine include the bypass fan, the core flow axial compressor, the

combustion chamber, the turbine, the mixer, and the nozzle. The incoming air is split into two parts after passing through the fan, with one part flowing through the bypass and the other part entering the core. The warm flow enters the compressor, where it is compressed and pressurized. The compressed air then enters the combustion chamber, where its temperature and entropy increase due to the reaction with fuel. The high-energy flow enters the turbine, where its temperature and pressure decrease. The flow then enters the mixer, where it is mixed with the cooler bypass flow, and finally exits through the nozzle. The thrust is generated through the reaction resulting from the discharge of the turbine's exhaust gases into the environment, proportional to the velocity and pressure of the flow at the nozzle exit and the ambient pressure [1]. Another type of air-breathing engine is the Ramjet. Ramjet engines, similar to gas turbine engines, operate based on the Brayton cycle. However, in ramjet engines, due to the high inlet Mach number, the entire compression process is achieved through aerodynamic compression in the inlet and diffuser. Thus, rotating components are absent in ramjet engines. In these engines, air is first compressed by the high-speed inlet, and then further compressed and heated in the diffuser. The heated air enters the burner, reacts with fuel, and exits the nozzle, where it expands and increases its velocity before being discharged into the environment, generating thrust in response to the discharge reaction [2–4]. The thermodynamic analysis of a gas turbine power plant [5] shows that the ratio of compression and ambient air temperature have a significant impact on the thermal efficiencies , resembling isentropic efficiencies. It's observed that thermal efficiency and output power decrease directly with an increase in the ambient air temperature. Additionally, specific fuel consumption and heat rate increase with an increase in the ambient air temperature [6].

Thermodynamic analysis and optimization of gas turbine engines have been conducted as advanced turbojets. It's observed that specific thrust is strongly dependent on the Turbine Inlet Temperature (TIT), such that a 10% reduction in TIT leads to a 6.7% reduction in specific thrust and a 6.8% reduction in specific fuel consumption. Furthermore, the optimum values for turbojets are determined at a flight altitude of 13000 meters and a Mach number of 0.8, with a compression ratio of 14 and TIT of 1700 K [7]. Optimization of a micro gas turbine engine's performance has also been carried out to maximize specific thrust and minimize specific fuel consumption. The results show that both specific fuel consumption and specific thrust of the turbojet engine are highly dependent on TIT and the compressor pressure ratio [8]. Furthermore, the effect of Mach number on the performance of a small turbojet engine, acting as a propulsive means for an unmanned aerial vehicle, has been studied. The analysis was conducted at a constant flight altitude of 8000 meters and a Mach number range of 0.3 to 0.8. The results show that within the Mach number range of 0.3 to 0.8, the exit thrust efficiency varies from 48.61% to 49.88%, and the exit energy efficiency varies from 3.25% to 9.96%. The efficiencies for the compressor, burner, and turbine were also evaluated. It was found that the exit thrust efficiency and exit energy efficiency both increase with an increase in the Mach number [9]. Optimization using the Particle Swarm Optimization (PSO) algorithm has been carried out for the J85 GE21 turbojet engine in the altitude range of 1000 to 8000 meters and a flight speed of 200 meters per second. In this study, the compressor pressure ratio, Mach number, and isentropic efficiencies of the nozzle, turbine, and compressor were taken as design parameters. The results showed the highest exit thrust efficiency among the engine components in various flight conditions was 73.1%, and the diffuser efficiency was also calculated [10]. A tool for thermodynamic analysis and optimization of gas turbine cycles called pyCycle has been developed. This tool can calculate thermodynamic cycle data with an error of 0.03% compared to the results obtained from the NPSS program [11]. Furthermore, energy and exergy optimization of a dual-shaft turbofan engine using the genetic algorithm has been performed. The TurboJet-Engine Optimizer v1 program was used for thermodynamic property calculations and optimization [12].

In another study, an exergy analysis of different components of the J85 GE21 turbojet engine was performed for Mach numbers of 0.4, 0.6, and 0.8. An analytical parameter was used to find the main parameters affecting efficiency. It was observed that TSFC increases with an increase in the Mach number [13]. In another study, the economic performance of a turbojet engine in off-design conditions has been investigated. In this study, an exergetic efficiency of 50.13% has been calculated [14]. Furthermore, the optimization of a gas turbine power cycle has been carried out with the objective of maximizing thermal efficiency, maximizing net power output, and minimizing specific engine speed with design variables including the compression ratio, inlet temperature of the turbine, and ambient air temperature [15]. Another study examined the effect of bypass ratio on the optimal fan pressure ratio in a turbofan engine. The Trent XBW engine series was investigated in this study, and the results indicated that increasing the bypass ratio leads to a decrease in specific fuel consumption and an increase in thrust [16]. Additionally, another paper explored the parametric study of a turbofan engine with high bypass ratio [17]. In another investigation, the performance of a turbofan engine with an inter-turbine burner was examined, and the impact of bypass ratio variations on the engine's performance was assessed [18]. Furthermore, an aerothermodynamic analysis of mixed-flow turbofan engines has been conducted [19]. Another study focused on analyzing the effects of compressor pressure ratio, fan pressure ratio, and turbine exit temperature on the performance of mixed-flow turbofan engines [20]. Additionally, the performance of a supersonic turbofan engine with a high bypass ratio was studied [21]. A study analyzed the thermodynamic and economic performance of turbojet and turbofan engines, as well as variable cycle engines for high-speed aircraft. The effects of turbine inlet temperature, compressor pressure ratio, altitude, and Mach number on thrust and specific fuel consumption were investigated [22]. Another research analyzed the thermodynamic performance of a hydrogen-fueled turbofan engine, showing that using hydrogen fuel instead of fossil fuels increases specific thrust and reduces specific fuel consumption under equivalent conditions [23]. Furthermore, a thermodynamic optimization of a turbofan engine cycle was performed considering various objective functions related to specific fuel consumption, overall compression ratio, fan compression ratio, and turbine inlet temperature [24]. A study focused on the conceptual design and optimization of a turbofan engine for supersonic commercial jets [25]. Another study conducted a thermodynamic analysis of a turbofan engine with a high bypass ratio (Trent 1000-A), revealing that increasing the overall pressure ratio enhances overall and thermal efficiency while reducing bypass ratio diminishes specific fuel consumption and increases specific thrust [26]. Moreover, an analysis of a ramjet engine's performance was carried out across a wide range of operating conditions [27].

In addition, a method for analyzing the performance of a ramjet engine was developed [28]. Another study investigated the thermodynamic efficiency and thrust of turbofan engines with combustion in a subsonic regime [29]. The effect of inlet air temperature on the performance of a gas turbine was studied, considering the influence of inlet temperature variations on compressor efficiency [30]. An economic and thermal analysis of a gas turbine using inlet air cooling was performed [31]. A study analyzed the exergy of a gas turbine engine (GE-F5) with inlet air cooling, showing that for each degree Celsius reduction in inlet air temperature within the range of 14 to 50 degrees Celsius, thermal efficiency and power output increase by 0.085% and 0.16 megawatts, respectively [32].

In this study, the influence of inlet air temperature [33] perturbations on turbojet, turbofan, mixed-flow, and ramjet engines at various altitudes and Mach numbers was initially investigated. Based on the results of this investigation and similar studies, optimization of the engines was performed using various objective functions. Due to the operational advantages of high-altitude flight and the reduction in air density with increasing altitude, leading to reduced dynamic pressure at constant speeds, the thermodynamic cycles of mixed-flow turbofan engines were modeled for different engines, including

F135PW100, EJ200, J85 GE21 turbojets, and XRJ47-W-5 ramjet, using GASTURB 10 software. The results of the modeling were validated against reference data. The optimization was performed using a genetic algorithm and MATLAB 10 software in two phases for three separate objective functions. The results were compared using the Tabu Search algorithm, and the superior cycle designs were selected based on J85 GE21 and F135PW100, EJ200 engines for the two phases of cycle design. Additionally, the impact of inlet air temperature perturbations on turbojets, turbofans, mixed-flow, and ramjet engines at various altitudes and Mach numbers was initially investigated. Considering the results of this investigation and similar studies, the engines were optimized using various objective functions.

2. Engines

- *F135 PW100 engine*

The F135 PW100 engine is a twin-spool mixed-flow turbofan engine with a bypass ratio designed for both subsonic and supersonic combustion. The main components of this engine include a three-stage axial flow fan, a six-stage axial flow compressor, an annular combustion chamber with the capability of afterburning, a high-pressure axial flow turbine, and two low-pressure axial flow turbines, as well as a nozzle. This engine is manufactured by PRATT AND WHITNEY and is utilized as the propulsion system for the LOCKHEED MARTIN-F35 LIGHTNING aircraft. In this study, the non-afterburning mode of this engine was considered [4]. The schematic of the F135 PW100 engine is depicted in Figure 1 [4].

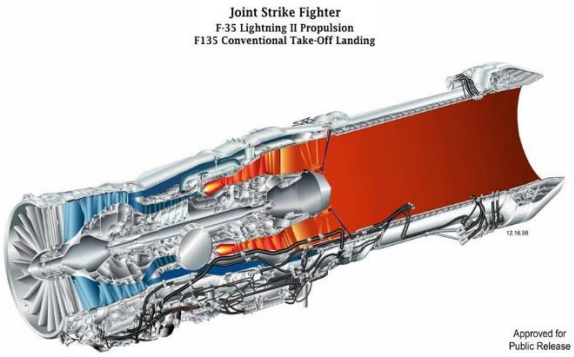

Fig. 1. Schematic diagram of F135 PW100 engine

- Engine EJ200

The EJ200 engine is a dual-shaft mixed-flow turbofan engine with a low bypass ratio and afterburning capability. Its main components include a three-stage axial fan, five-stage axial compressor, annular combustion chamber, featuring three stages of high-pressure axial turbines and five stages of low-pressure axial turbines, as well as a nozzle. This engine is produced by AERO JET TURBO GMBH and is used as the propulsion system for the EUROFIGHTER TYPHOON aircraft.

The schematic of the EJ200 engine is shown in Figure 2.

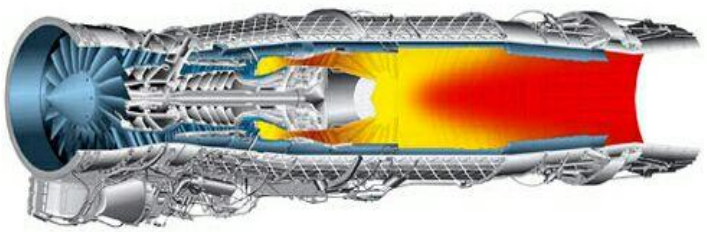

Fig. 2. Schematic diagram of EJ engine

- *Engine J85 GE17*

It is a single-shaft turbojet engine. Its main components include an 8-stage axial compressor, a 2-stage axial turbine, an annular combustion chamber, and a nozzle. This engine is manufactured by General Electric and is utilized as the propulsion system for the Northrop F5 fighter aircraft.

- *XRJ47-W-5 engine*

An American ramjet engine manufactured by WRIGHT AERONAUTICAL. This engine has been utilized as the propulsion system for the SM64 Navaho cruise missile.

Schematic cycle of J85GE21 turbojet, F135 PW100 turbofan, EJ200 turbofan, and XRJ47-W-5 ramjet engines, along with their inlet air cooling system. Flow diagram of a mixed-flow turbofan engine with an inlet air cooling system is shown in Fig. 3.

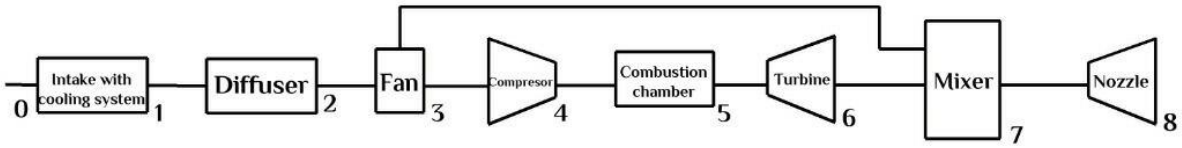

Fig. 3. flow chart of turbofan engine with mixed flow with air intake cooling system.

The turbojet engine flow chart with the intake air cooling system is shown in Figure 4.

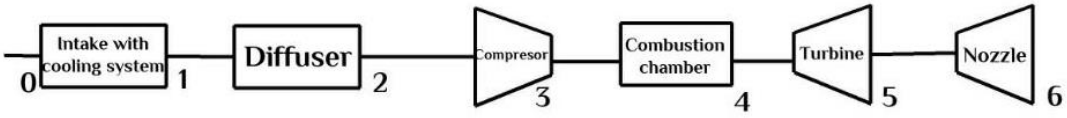

Fig. 4. flow chart of turbojet engine with intake air cooling system.

The flow diagram of the ramjet engine with the intake air cooling system is shown in Figure 5.

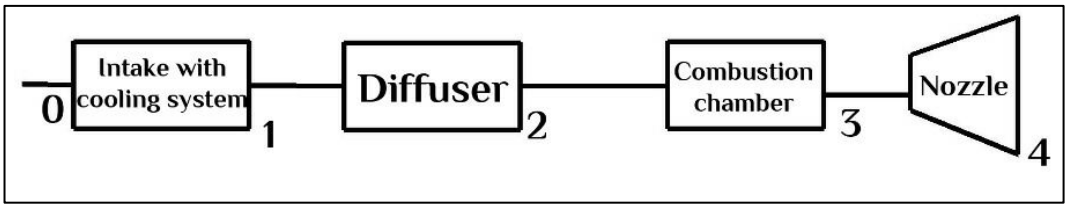

Fig. 5. Flow diagram of Ramjet engine with air intake cooling system

This study focuses on the investigation of a dual-shaft mixed-flow turbofan engine (F135PW100), a dual-shaft mixed-flow turbofan engine EJ200, a single-shaft turbojet engine J85 GE17, and a ramjet engine XRJ47-W-5. Figure 1 illustrates schematics of the engines under study. Figure 2 depicts the flow diagram of the dual-shaft mixed-flow turbofan engine with inlet air cooling system, along with a turbojet engine and a ramjet engine, both equipped with inlet air cooling systems.

Thermodynamic and thermal modeling are conducted as part of this study.

2.1. Turbojet Equations

The changes in air flow pressure at the intake and cooling system is negligible:

$$P_0 = P_1 \tag{1}$$

$$T_1 = T_0 + \Delta T \tag{2}$$

P_0 and T_0, respectively, ambient air pressure and ambient air temperature and P_1 and T_1, respectively, are diffuser inlet pressure and diffuser inlet temperature, P_2 and T_2, respectively are the fan inlet pressure and fan inlet temperature and ΔT is the temperature difference between diffuser inlet to ambient.

Assuming the diffuser is isentropic, diffuser exit air temperature is calculated as follows;

$$T_2 = T_1\left(1 + \frac{k_d - 1}{2} M_a^2\right) \tag{3}$$

where T_1 and T_2 are exit and inlet air temperature to the diffuser.k_d is Specific heat at constant pressure to specific heat in constant volume for air passing through the diffuser, which is a function of the average temperature of the air passing through flight Mach number. M_a is flight mach number. The exiting air pressure of the diffuser is calculated as follows;

$$P_2 = P_1\left(\frac{T_2}{T_1}\right)^{\frac{k_d}{k_d - 1}} \tag{4}$$

Where P_1 and P_2 are air pressure at exit and inlet of the diffuser, respectively; and T_1 and T_2 are exit and inlet air temperature to the diffuser. k_d specific heat at constant pressure to specific heat in constant volume for passing air of diffuser which is calculated as a function of the average temperature of the passing air of the diffuser. Assuming air and fuel combustion products with air are ideal gas. The compressor exit pressure is obtained from the following equation;

$$P_{3=\pi_c} P_2 \tag{5}$$

π_c is compressor pressure ratio and $P_3$is compressor exit pressure and $P_2$is fan exit air pressure The exit temperature of compressor is obtained as follow

$$T_3 = \frac{T_2}{\eta_C}\left[\left(\frac{P_3}{P_2}\right)^{\frac{k_c - 1}{k_c}} - 1\right] + T_2 \tag{6}$$

where η_c is compressor isentropic efficiency and T_3 is compressor exit air temperature and T_2 is fan exit air temperature and K_c is specific heat at constant pressure to specific heat in constant volume for passing air of fan is calculated as a function of the average air passing. Engine intake air real mass flow rate is calculated as follow;

$$m_a = \rho V_0 A \tag{7}$$

where A is cross section of real air inlet flow and ρ is density of inlet air flow and $V_0$is flight velocity. Flight velocity is calculated in which;

$$V_0 = M_a(RkT_0)^{0.5} \tag{8}$$

that M_a is the flight mach number, R is the global constant gas, and k is the ratio of specific heat at constant pressure to specific heat at constant volume of air is calculated as a function of the ambient air temperature. V_0 is also the flight velocity.

Compressor power is obtained as follows;

$$W_C = m_a \frac{T_2}{\eta_C}\left[\left(\frac{P_3}{P_2}\right)^{\frac{k_c-1}{k_c}} - 1\right] + T_2 \tag{9}$$

where W_C is compressor power consumption and $\eta_C$is compressor isentropic efficiency and K_c is specific heat at constant pressure to specific heat in constant volume ratio is calculated as a function of the average of compressor air temperature.m_a is real air mass flow rate. Combustion chamber exit pressure is obtained as follow;

$$P_4 = P_3 - \Delta P_{combustor} \tag{10}$$

where P_4 is combustion chamber exit pressure P_3 is compressor inlet pressure.

$\Delta P_{combustor}$ is pressure drop in the combustion chamber is evaluated as a percentage of the air exit pressure of compressor. Heat rate is calculated as follow;

$$Q_h = m_a C_{av}(T_4 - T_3) \tag{11}$$

where Q_h is heat rate and $C_{av}$is specific heat at constant pressure is calculated as a function of average flow temperature in the combustion chamber. Also, $T_3$is inlet air temperature of turbine and $T_4$is inlet air temperature of turbine. Fuel mass flow rate is calculated as follow;

$$m_f = \frac{Q_h}{FHV\ \eta_{combustor}} \tag{12}$$

where FHV is fuel heat value per kilograms and $\eta_{combustor}$ is combustion efficiency at combustion chamber and m_f is fuel consumption and $Q_h$is heat rate. Turbine intake mass flow rate is calculated as follow;

$$m_T = m_a + m_f \tag{13}$$

where m_f is fuel consumption rate and $m_a$is real air mass flow rate.

Turbine power is calculated as follow;

$$W_T = m_T . C_{Pavt} . (T_4 - T_5) \tag{14}$$

where m_T is turbine inlet mass flow rate and C_{pav} is specific heat at costant pressure which is obtained as a function of the average temperature in the turbine.

Assuming that mechanical power losses in the spools is negligible, according to the energy conservation law, the turbine power is equal to the compressor power.

$$m_T.C_{Pavt}.(T_5 - T_6) = m_a\left[\frac{T_2}{\eta_C}\left[\left(\frac{P_3}{P_2}\right)^{\frac{k_c-1}{k_c}} - 1\right] + T_2\right] \quad (15)$$

In which T_5 is the turbine exit temperature and T_4 is the turbine inlet temperature, m_T is the turbine mass flow rate and C_{pavt} is the specific heat at costant pressure, which is obtained as a function of the average temperature during the turbine. η_c is also the compressor isentropic efficiency. Also, k_c is the ratio of specific heat at constant pressure to specific heat of the same volume as air, which is calculated as a function of the average air temperature during compressor. By obtaining the turbine exit temperature of the equation (17), the turbine exit pressure is calculated as follows:

$$P_5 = P_4\left[1 - \frac{1}{\eta_t}\left(1 - \frac{T_5}{T_4}\right)\right]^{\frac{k_t}{k_t-1}} \quad (16)$$

T_5 is the output temperature of the turbine, T_4 is the inlet temperature of the turbine, and $P_5$and P_4, respectively, are the turbine exit pressure and turbine inlet pressure. k_t is the ratio of specific heat at constant pressure to specific heat at constant volume, which is a function of the average temperature during the turbine, and η_T is the turbine isentropic efficiency.

The flow pressure at the nozzle exit is obtained.

$$P_6 = P_5\left[1 - \frac{1}{\eta_n}\left(1 - \left(\frac{T_6}{T_5}\right)\right)\right]^{\frac{K_n}{K_n-1}} \quad (17)$$

that P_6 is the flow pressure at the output nozzle and T_6 is the flow temperature at the output nozzle and K_n is the ratio of specific heat at constant pressure to hot stream nozzle exit, which is obtained as a function of the average temperature along the stream nozzle and $\eta_n$is the nozzle isentropic efficiency.

The nozzle exit velocity is obtained in such a way;

$$V_6 = \left(2\eta_n\frac{K_n}{K_n - 1}.R.T_6\left[1 - \left(\frac{P_6}{P_5}\right)^{\frac{K_n-1}{K_n}}\right]\right)^{0.5} \quad (18)$$

that K_n is the ratio of specific heat at cost constant pressure to specific heat at constant valume, which is a function of the average temperature during nozzle and R is the global gas constant, P_7 is the nozzle exit pressure. thrust is calculated in such a way;

$$F = \frac{1}{g_c}\left[\left((m_a + m_f)(V_6)\right) - (m_a V_0)\right] + [A_6(P_6 - P_0)] \quad (19)$$

that A_6 is the nozzle exit area, P_0 is the ambient air pressure, V_0 is the flight speed, and g_c is the gravity of the earth and F is the thrust force, and m_a is the real air mass flow rate. The specific fuel consumption is equal to the ratio of fuel mass flow rate to thrust force,

$$TSFC = \frac{m_f}{F} \quad (20)$$

in which TSFC is the specific fuel consumption. Thermal efficiency is calculated in such a way;

$$\eta_{th} = \frac{m_T(V_6^2 - V_0^2)}{2m_f FHV} \tag{21}$$

that η_{th} is the thermal efficiency of the engine and m_T is the turbine exit mass flow rate. Propulsive efficiency is calculated in such a way;

$$\eta_P = \frac{V_0 F}{m_T(V_6^2 - V_0^2)} \tag{22}$$

that η_P is the propulsion efficiency of the engine and m_T is the mass flow rate.

2.2. Mixed flow turbofan Equation

The thermodynamic and thermal modeling equations of the mixing flow turbofan are shown in Table 1.

Table 1. of thermodynamic and thermal modeling equations of mix flow turbofan

$$P_0 = P_1$$

$$T_1 = T_0 + \Delta T$$

$$T_2 = T_1\left(1 + \frac{k_d - 1}{2} M_a^2\right)$$

$$P_{3=\pi_{fan}} P_2$$

$$T_3 = \frac{T_2}{\eta_{fan}}\left[\left(\frac{P_3}{P_2}\right)^{\frac{k_f - 1}{k_f}} - 1\right] + T_2$$

$$P_{4=\pi_C} P_3$$

$$T_4 = \frac{T_3}{\eta_C}\left[\left(\frac{P_4}{P_3}\right)^{\frac{k_c - 1}{k_c}} - 1\right] + T_3$$

$$m_{total} = \rho V_0 A$$

$$m_{ah} = \frac{m_{total}}{\alpha + 1}$$

$$W_C = m_{ah}\frac{T_3}{\eta_C}\left[\left(\frac{P_4}{P_3}\right)^{\frac{k_c - 1}{k_c}} - 1\right]$$

$$W_T = m_T . C_{Pavt} . (T_5 - T_6)$$

$$P_6 = P_5\left[1 - \frac{1}{\eta_t}\left(1 - \frac{T_6}{T_5}\right)\right]^{\frac{k_t}{k_t - 1}}$$

$$T_7 = \frac{T_6 C_{P6} m_{ah+(m_{ac} C_{P3} T_3)}}{C_{P7}}$$

$$P_7 = RT_7$$

$$m_7 = m_{ah} + m_{ac} + m_f$$

$$P_8 = P_7\left[1 - \frac{1}{\eta_n}\left(1 - \left(\frac{T_8}{T_7}\right)\right)\right]^{\frac{K_n}{K_n - 1}}$$

$$V_8 = \left(2\eta_n \frac{K_n}{K_n - 1} RT_7\left[1 - \left(\frac{P_8}{P_7}\right)^{\frac{K_n - 1}{K_n}}\right]\right)^{0.5}$$

$$F = m_7(V_8 - V_0) + A_8(P_8 - P_0)$$

$$TSFC = \frac{m_f}{F}$$

$$W_{fan} = m_{ac}\frac{T_2}{\eta_{fan}}\left[\left(\frac{P_3}{P_2}\right)^{\frac{k_f-1}{k_f}} - 1\right] \qquad \eta_{th} = \frac{m_7(V_8^2 - V_0^2)}{2m_f FHV}$$

$$m_{ac} = m_{total} - m_{ah} \qquad \eta_P = \frac{V_0 F}{m_7(V_8^2 - V_0^2)}$$

$$P_5 = P_4 - \Delta P_{cambustor}$$

$$Q_h = m_{ah}C_{av}(T_5 - T_4)$$

$$m_f = \frac{Q_h}{FHV\ \eta_{combustor}}$$

$$m_T = m_{ah} + m_f$$

where m_{total} is the total mass flow rate of the inlet air, and m_{ah} and m_{ac} are the mass flow rates of the inlet air to the compressor and the mass flow rate of air to the afterburner, respectively. Additionally, ρ, V_0, and A represent the ambient air density, flight velocity, and inlet channel cross-sectional area of the engine, respectively. Moreover, α stands for the bypass ratio of the engine. π_{fan} and η_{fan} denote the total pressure ratio across the fan and the isentropic fan efficiency, respectively. Similarly, π_C and η_C represent the total pressure ratio across the compressor and the isentropic efficiency of the compressor, respectively. T_4 corresponds to the temperature of the exhaust flow from the burner. T_7 and P_7 respectively indicate the pressure and temperature of the flow at the mixer exit, and T_8 and P_8 correspond to the temperature and pressure of the flow at the nozzle exit.

2.3. Ramjet equations

The changes in air flow pressure at the intake and cooling system is negligible:

$$P_0 = P_1 \tag{23}$$

$$T_1 = T_0 + \Delta T \tag{24}$$

P_0 and T_0, respectively, ambient air pressure and ambient air temperature and P_1 and T_1, respectively, are diffuser inlet pressure and diffuser inlet temperature, P_2 and T_2, respectively are the fan inlet pressure and fan inlet temperature and ΔT is the temperature difference between diffuser inlet to ambient.

Assuming the diffuser is isentropic, diffuser exit air temperature is calculated as follows.

$$T_2 = T_1\left(1 + \frac{k_d - 1}{2}M_a^2\right) \tag{25}$$

where T_1 and T_2 are exit and inlet air temperature to the diffuser.k_dSpecific heat at constant pressure to specific heat in constant volume for air passing through the diffuser, which is a function of the average temperature of the air passing through flight Mach number. M_a is flight mach number. The exiting air pressure of the diffuser is calculated as follows;

$$P_2 = P_1\left(\frac{T_2}{T_1}\right)^{\frac{k_d}{k_d-1}} \tag{26}$$

where P_1 and P_2 are air pressure at exit and inlet of the diffuser, respectively; and T_1 and T_2 are exit and inlet air temperature to the diffuser. k_d specific heat at constant pressure to specific heat in constant volume

for passing air of diffuser which is calculated as a function of the average temperature of the passing air of the diffuser. Assuming air and fuel combustion products with air are ideal gas. Combustion chamber exit pressure is obtained as follow;

$$P_3 = P_2 - \Delta P_{combustor} \tag{26}$$

where P_3 is combustion chamber exit pressure P_2 is compressor inlet pressure.

$\Delta P_{combustor}$ is pressure drop in the combustion chamber. Heat rate is calculated as follow;

$$Q_h = m_a C_{av}(T_3 - T_2) \tag{27}$$

where Q_h is heat rate and $C_{av}$is specific heat at constant pressure is calculated as a function of average flow temperature in the combustion chamber. Also, T_2 is inlet air temperature of turbine and $T_3$is inlet air temperature of nozzle. Fuel mass flow rate is calculated as follow;

$$m_f = \frac{Q_h}{FHV\ \eta_{combustor}} \tag{28}$$

where FHV is fuel heat value per kilograms and $\eta_{combustor}$ is combustion efficiency at combustion chamber and m_f is fuel consumption and $Q_h$is heat rate. Nozzle inlet mass flow rate is calculated as follow;

$$m_T = m_a + m_f \tag{28}$$

where m_f is fuel consumption rate and m_a is hot stream real air mass flow rate. The flow pressure at the nozzle exit is obtained.

$$P_4 = P_3 \left[1 - \frac{1}{\eta_n}\left(1 - \left(\frac{T_4}{T_3}\right)\right)\right]^{\frac{K_n}{K_n - 1}} \tag{29}$$

that P_4 is the flow pressure at the output nozzle and $T_4$is the flow temperature at the output nozzle and Kn is the ratio of specific heat at costant pressure to nozzle exit, which is obtained as a function of the average temperature along the nozzle and η_n is the nozzle isentropic efficiency.

The nozzle exit velocity is obtained in such a way;

$$V_4 = \left(2\eta_n \frac{K_n}{K_n - 1}.R.T_4\left[1 - \left(\frac{P_4}{P_3}\right)^{\frac{K_n - 1}{K_n}}\right]\right)^{0.5} \tag{29}$$

that K_n is the ratio of specific heat at cost constant pressure to specific heat at constant valume, which is a function of the average temperature during nozzle and R is the global gas constant, P_4 is the nozzle exit pressure. thrust is calculated in such a way;

$$F = \frac{1}{g_c}\left[\left(\left(m_a + m_f\right)(V_4)\right) - (m_a V_0)\right] + [A_4(P_4 - P_0)] \tag{30}$$

that A_6 is the nozzle exit area, P_0 is the ambient air pressure, V_0 is the flight speed, and g_c is the gravity of the earth and F is the thrust force, and m_a is the real air mass flow rate. The specific fuel consumption is equal to the ratio of fuel mass flow rate to thrust force;

$$TSFC = \frac{m_f}{F} \tag{31}$$

in which TSFC is the specific fuel consumption.

Propulsive efficiency is calculated in such a way;

$$\eta_P = \frac{V_0 F}{m_T(V_4^2 - V_0^2)} \tag{32}$$

that η_P is the propulsion efficiency of the engine and m_T is the mass flow rate.

TSF is calculated in such a way;

$$TSF = \frac{F}{m_{total}} \tag{33}$$

that F is thrust force and m_{total} is intake real air mass flow rate.

Another parameter called Thrust per Dynamic Pressure ($TPDP$) ratio as a measure of engine acceleration ability is equal to the thrust force ratio to the dynamic pressure of the air flow around the aircraft.

$$TPDP = \frac{2F}{\rho_0 \, V_0^2} \tag{34}$$

where ρ_0 is the ambient air density and V_0 is the flight speed and F is the thrust force. For turbine engines the nitrogen oxides emission index coefficient (SNOx) is obtained in such a way

$$S_{nox} = \left(\frac{P_4}{2965kPa}\right)^{0.4} e^{\left(\frac{T_4 - 826K}{194K} + \frac{6.29 - (100.war)}{53.2}\right)} \tag{35}$$

that T_4 and P_4, respectively, are the compressor exit air temperature and compressor exit air pressure and war is the ratio of liquid water air to the compressor exit air. In this study, the effect of fuel type and combustor geometry on the index of production intensity of SNOx has been omitted and only the effect of temperature, pressure and liquid water air ratio of the incoming air on it has been discussed.

Also, the parameter of the emission coefficient of nitrogen oxides EI NOx is calculated as follows;

$$EI_{NO_x} = 23SNOx \tag{36}$$

where EI_{NO_x} is the emission parameter of nitrogen oxides.

Table 2. Thermodynamic cycle input parameters of three engines F135PW100, EJ200, J85 GE21

	F135 PW 100 turbofan	***EJ200 turbofan***	***J85 GE17 turbojet***
$T_{inlet\ turbine}$	2175(K)	1800(K)	1139(K)
Overall compressor pressure ratio	28.2	26	7

$Fan\ pressure\ ratio$	5.1	4.2	-
$Bypass\ ratio$	0.57	0.4	-
$\dot{m}_{air}$	147(Kg/s)	77(Kg/s)	20(Kg/s)
$\eta_{is,fan}$	0.90	0.90	0.87
$\eta_{is,compressor}$	0.85	0.85	0.9

Table 3. Thermodynamic cycle input parameters of XRJ47-W5 engine.

Parameters	**Values**
Burner exit temperature	2300(K)
Burner inlet Mach number	0.2
Air mass flow rate	55(Kg/s)
$\eta_{is,nozzle}$	0.92

Table 4. Fuel heat value of considered fuels [16-21]

Fuel heat value	Hydrogen	Natural gas	JP10
	118 (Mj/kg)	49.736 (Mj/kg)	42.076 (Mj/Kg)

3. Validation

In this study, the GASTURB10 software was utilized for the thermodynamic cycle modeling. The cycle parameters of the EJ200, F135PW100, J85GE17 engines are presented in Table 5, and for the XRJ47-W-5 engine in Table 5. The heating values of the fuels are shown in Table 5. To validate the conducted modeling, the calculated values for thrust and TSFC were compared against reference values for the F135PW100, EJ200, and J85 GE17 engines under sea level static conditions (Ma=0, H=0), and for the XRJ47-W-5 engine under specific conditions (Ma=2.75, H=18333m) using JP10 fuel. The obtained values for thrust and TSFC for the F135PW100, EJ200, and J85 GE17 engines under sea level static conditions and the XRJ47-W-5 engine under specific conditions, compared to the reference values, are shown in Table (). The percentage differences in thrust results are within the range of 2.97-12.33%, and for TSFC, they are within the range of 4.22-8%.

Table 5. comparison of trust force and TSFC with references in take-off mode.

		F135PW100	EJ200	J85 GE17	XRJ47-W-5
$Thrust(KN)$	$Reference\ value$	125.90	60	12.67	45
	$Present\ study$	122.16	63.28	12.52	39.45
	$diveation(\%)$	-2.97	5.46	1.18	12.33
$TSFC(g/KNs)$	$Reference\ value$	25	24	27	95
	$Present\ study$	27	23.971	23.733	87.507
	$diveation(\%)$	8	4.22	8.71	7.88

4. Results and Discussion

In this section, using the conducted thermodynamic modeling, the effect of variations in the inlet air temperature to turbojet, turbofan, and ramjet engines has been investigated at different Mach numbers and flight altitudes.

The variations in real air mass flow rate and thrust of J85GE21 turbojet, F135 PW100 turbofan, and EJ200 turbofan engines at a flight altitude of 20,000 meters and a Mach number range of 0.5 to 2.5, as well as the XRJ47-W-5 ramjet engine at a flight altitude of 20,000 meters and a Mach number range of 2.5 to 4, using JP10 fuel, are presented in Figure 6.

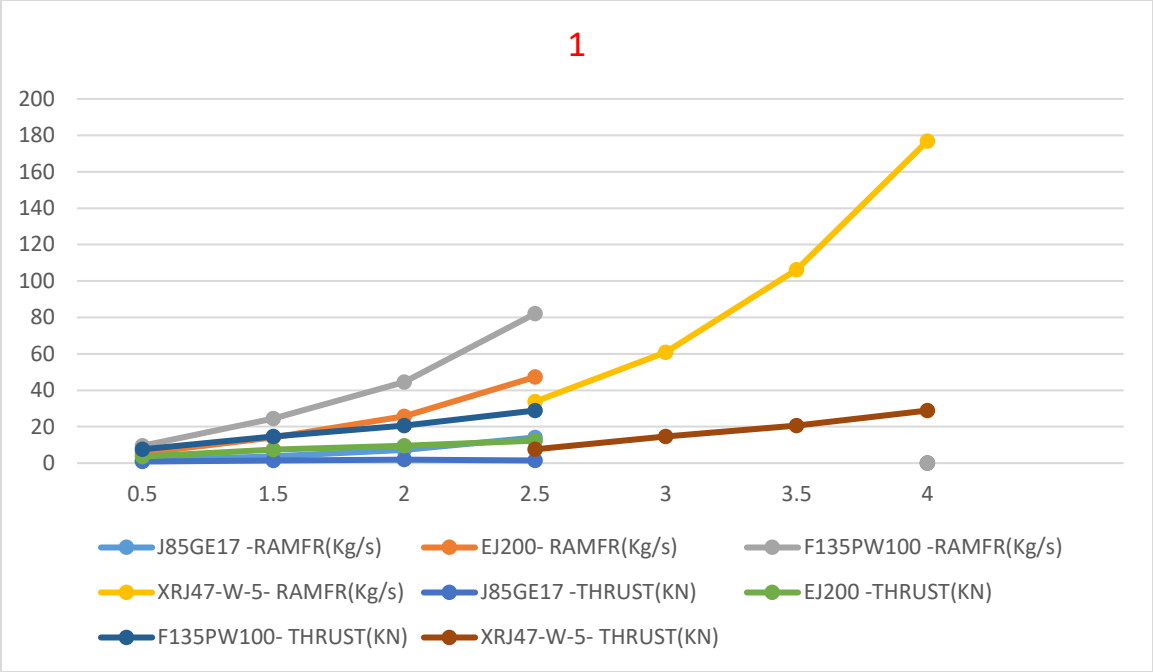

Fig. 6 the variations in real air mass flow rate and thrust of J85GE21 turbojet, F135 PW100 turbofan, and EJ200 turbofan engines at a flight altitude varied by Mach Number.

Fig. 7 illustrates the variations in real air mass flow rate and thrust of J85GE21 turbojet, F135 PW100 turbofan, and EJ200 turbofan engines at a flight altitude of 20,000 meters and a Mach number range of 0.5 to 2.5, as well as the XRJ47-W-5 ramjet engine at a flight altitude of 20,000 meters and a Mach number range of 2.5 to 4, using JP10 fuel. Additionally, the variations in real air mass flow rate and thrust of J85GE17 turbojet, F135 PW100 turbofan, EJ200 turbofan, and XRJ47-W-5 ramjet engines at different Mach numbers within the flight altitude range of 10,000 to 30,000 meters, using JP10 fuel, are presented in Figure 8.

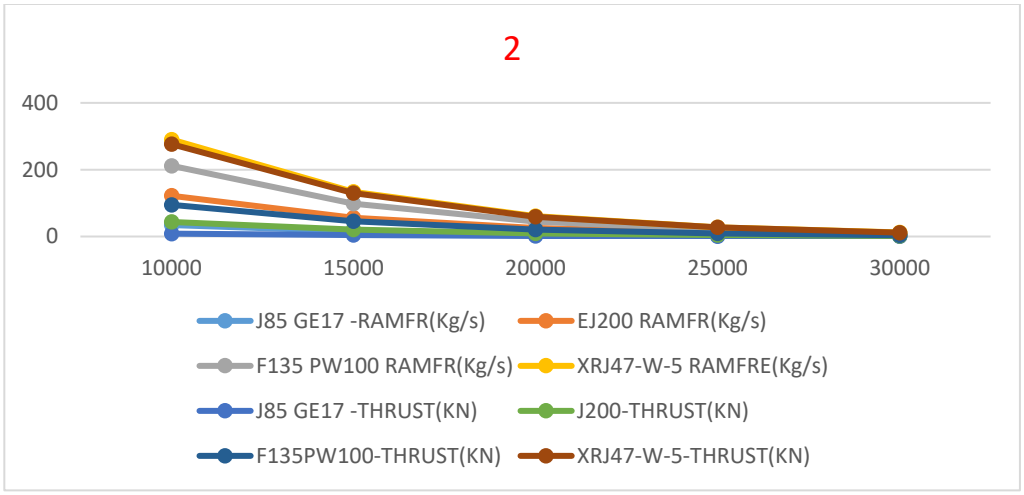

Figure 7. Real air mass flow rate and thrust variations for J85GE17 turbojet, F135 PW100 turbofan, EJ200 turbofan, and XRJ47-W-5 RAMJET engines at different flight altitudes within the range of 10,000 to 30,000 meters, considering various Mach numbers, using JP10 fuel.

As the results indicate, with an increase in the Mach number at a constant flight altitude, the true airspeed increases. An increase in true airspeed leads to an increase in the real air mass flow rate. On the other hand, at a constant Mach number, the density of the ambient air decreases with an increase in flight altitude. As the density of the ambient air decreases, the real air mass flow rate also decreases. Additionally, for the engines J85GE21 turbojet, F135 PW100 turbofan, EJ200 turbofan, and XRJ47-W-5 ramjet, at a constant altitude, an increase in the Mach number results in an increase in the real mass flow rate of incoming air to the engine. This increase in real air mass flow rate leads to an increase in engine thrust. However, at a constant Mach number, as the flight altitude increases, the real air mass flow rate decreases, consequently leading to a decrease in engine thrust.

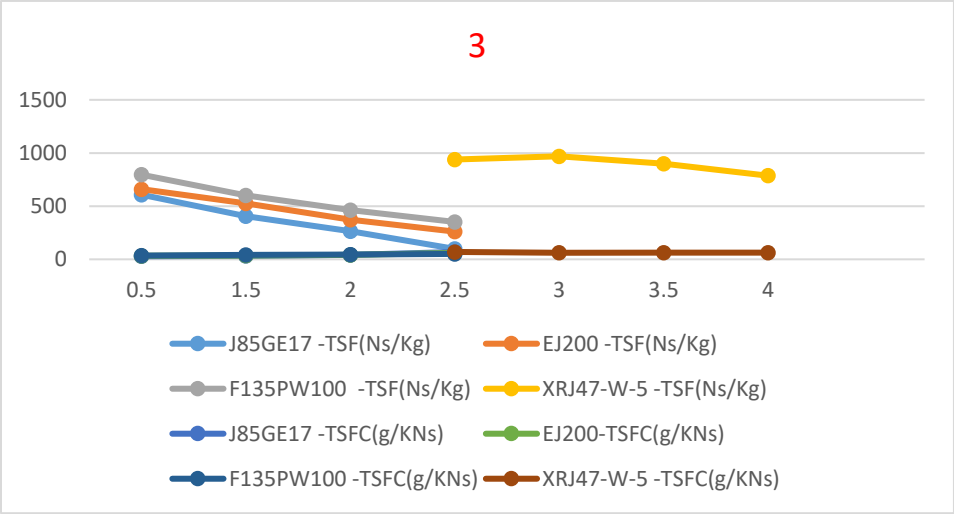

Fig. 8. TSFC and thrust-specific fuel consumption (TSF) variations for J85GE21 turbojet, F135 PW100 turbofan, EJ200 turbofan engines at an altitude of 20,000 meters, within the range of Mach numbers 0.5 to 2.5, and for XRJ47-W-5 RAMJET engine at an altitude of 20,000 meters, within the range of Mach numbers 2.5 to 4, using JP10 fuel

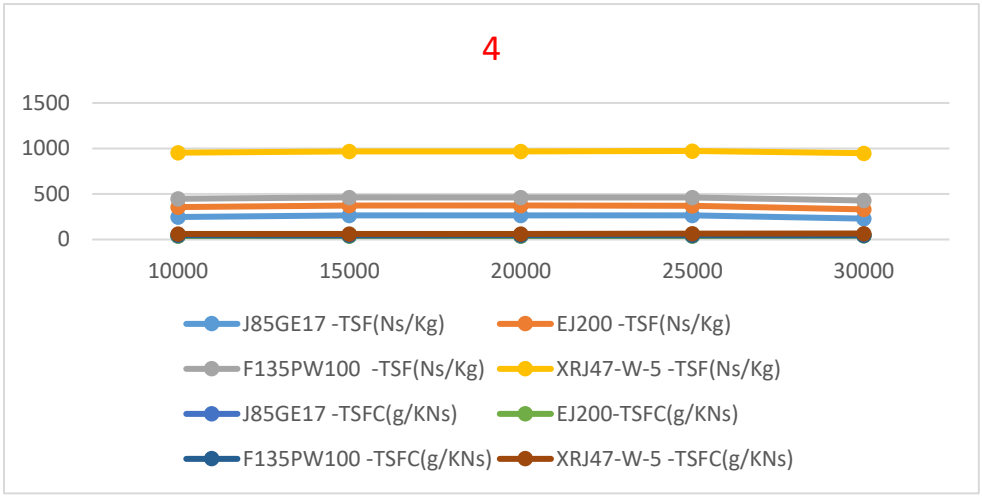

Fig. 8. TSFC and thrust-specific fuel consumption (TSF) variations for J85GE17 turbojet, F135 PW100 turbofan, EJ200 turbofan engines, and XRJ47-W-5 RAMJET engine, at altitudes ranging from 10,000 to 30,000 meters, within the range of Mach numbers, using JP10 fuel.

4.1. Effect of fuel types on performance

In the present discussion, the variations of Thrust and thrust-specific fuel consumption (TSFC) under specific conditions are analyzed for the F135PW100 and XRJ47-W-5 engines using different fuels: JP10, Natural Gas, and Hydrogen. The analysis is conducted at a Mach number of 2 and flight altitude of 10,000 meters for the F135PW100 engine and a Mach number of 3 and flight altitude of 10,000 meters for the XRJ47-W-5 engine.

The observations reveal that the molecular weight of combustion products resulting from fuel combustion with air is generally lower. With a decrease in molecular weight of the combustion products, the exit velocity of nozzle increases, subsequently raising the thermodynamic velocity of the thrust force. Consequently, the thermodynamic cycle using hydrogen fuel exhibits the highest thrust force due to the lower molecular weight of its combustion products.

Additionally, under equivalent conditions, an increase in the heating value of the fuel leads to a reduction in fuel mass flow rate, resulting in a decrease in TSFC. As a result, the cycle using hydrogen fuel demonstrates the lowest TSFC under these circumstances.

Furthermore, a decrease in molecular weight under equivalent conditions leads to an increase in thrust force, thereby causing an increase in TSF. This leads to the cycle with hydrogen fuel having the highest TSF under equivalent conditions due to its reduced molecular weight.

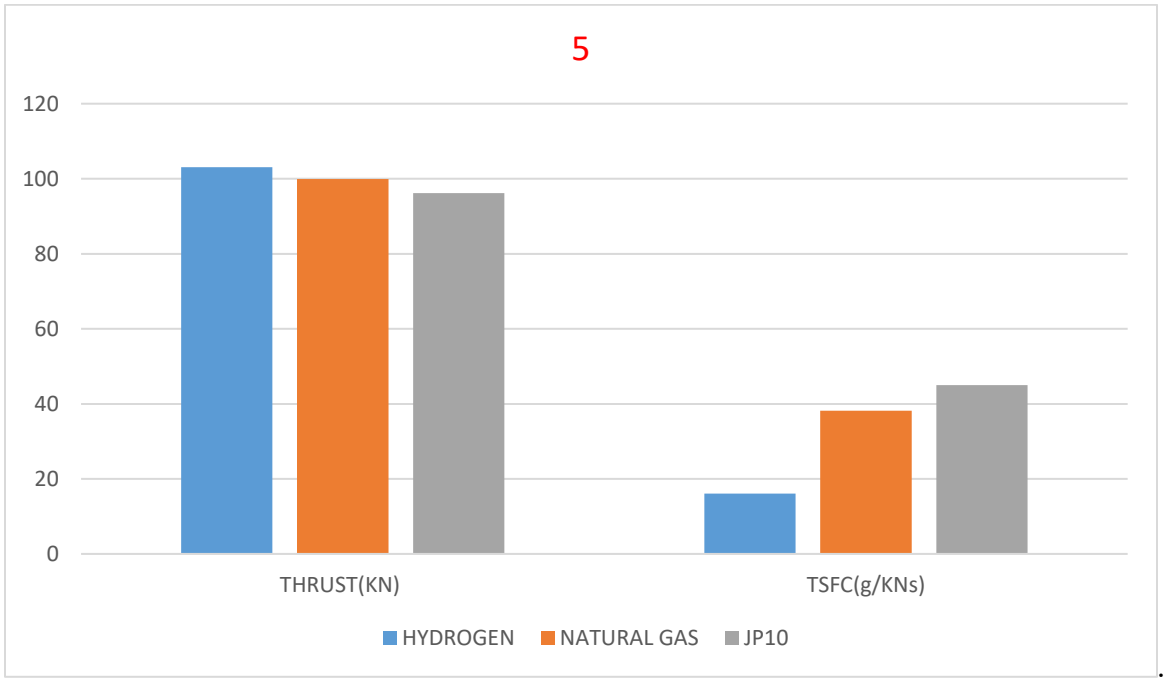

Fig. 9 Thrust and TSFC charts in the conditions of Mach 2 and altitude of 10000 meters for F135PW100 engine for JP10, Natural gas and Hydrogen fuels.

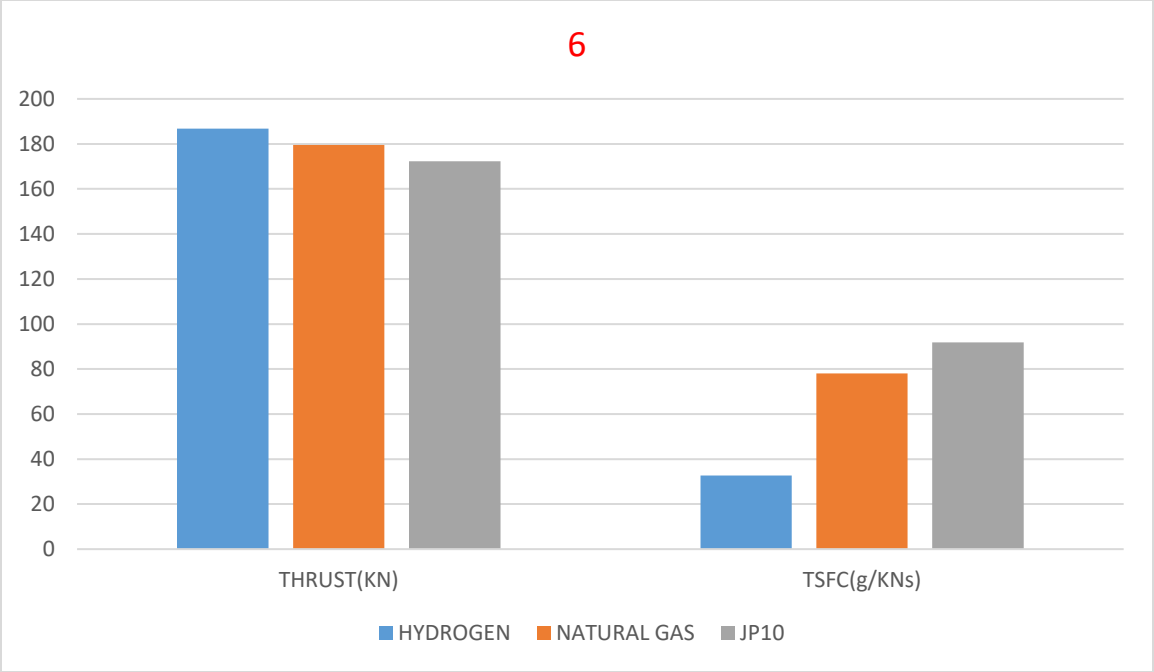

Fig. 10. Thrust and TSFC charts in the conditions of Mach 3 and altitude of 10000 meters for XRJ47-W-5 engine for JP10, Natural gas and Hydrogen fuels.

4.2. Effect of inlet air temperature changes on performance

In this study, the effect of changes in inlet air temperature on J85GE21 turbojet, F135 PW100 turbofan, EJ200 turbofan, XRJ47-W-5 ramjet engines for using hydrogen and jet fuel at an altitude of 20000 meters and different Mach has been investigated. The changes of the inlet air flow rate for J85GE17 turbojet, F135 PW100 turbofan, EJ200 turbofan, XRJ47-W-5 ramjet engines at an altitude of 20,000 meters and for hydrogen fuel are shown in Figure 11 for the inlet air temperature changes. J85GE17 turbojet, F135 PW100 turbofan, EJ200 turbofan, XRJ47-W-5 ramjet at any altitude and Mach, as the temperature of the inlet air decreases, the density of the inlet air increases, so the actual flow rate of the inlet air increases.

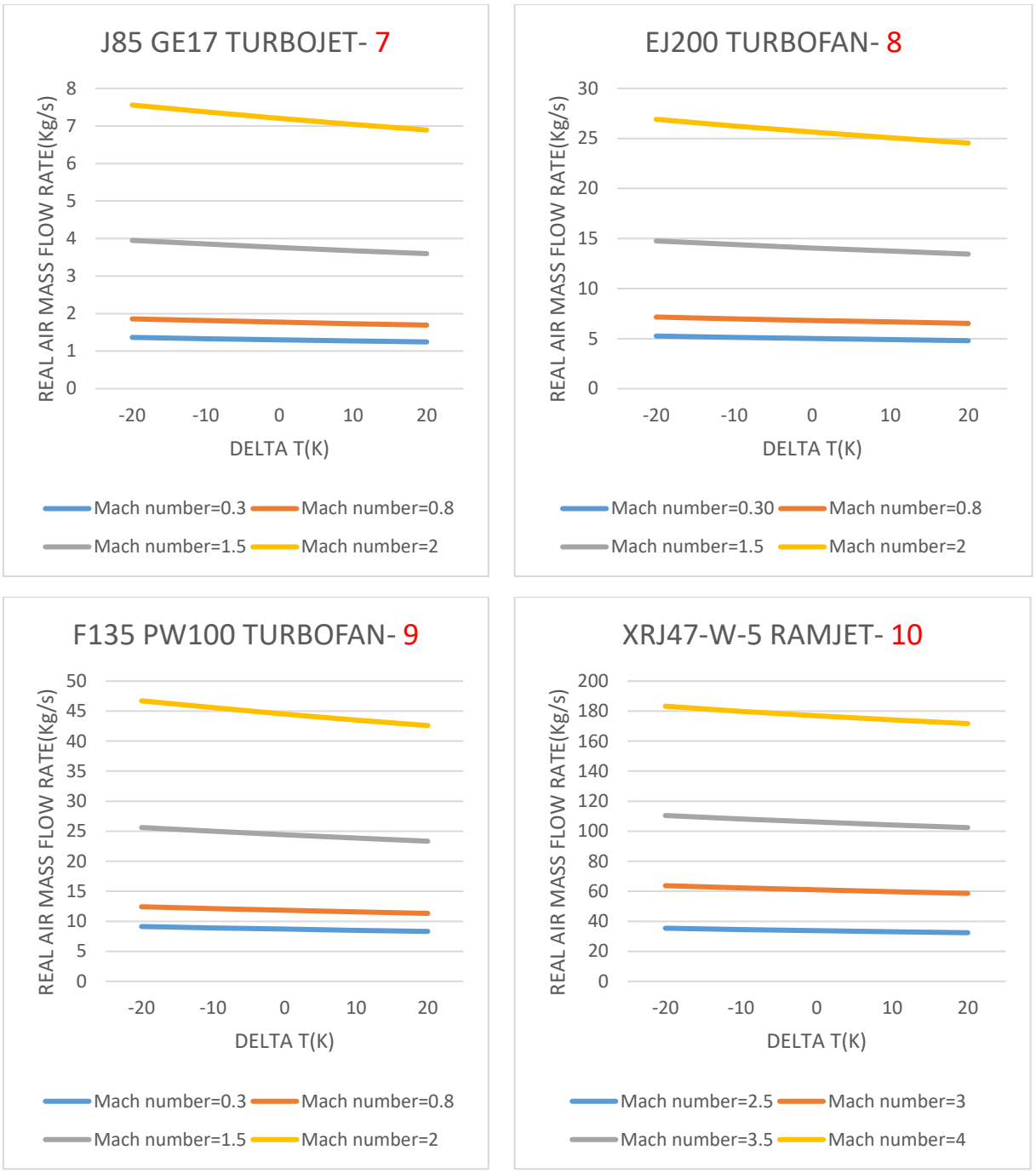

Fig. 11. changes in the actual flow rate of the inlet air for J85GE17 turbojet, F135 PW100 turbofan, EJ200 turbofan, XRJ47-W-5 ramjet engines at an altitude of 20,000 meters and for hydrogen fuel

Thrust changes for J85GE17 turbojet, F135 PW100 turbofan, EJ200 turbofan, XRJ47-W-5 ramjet engines at an altitude of 20,000 meters and for hydrogen fuel with changes in inlet air temperature are shown in Figure 12. For J85GE17 turbojet, F135 PW100 turbofan, EJ200 turbofan, XRJ47-W-5 ramjet engines, with the decrease of the inlet air temperature, the actual flow rate of the inlet air increases. Therefore, with the decrease of the inlet air temperature, the thrust of the engine also increases.

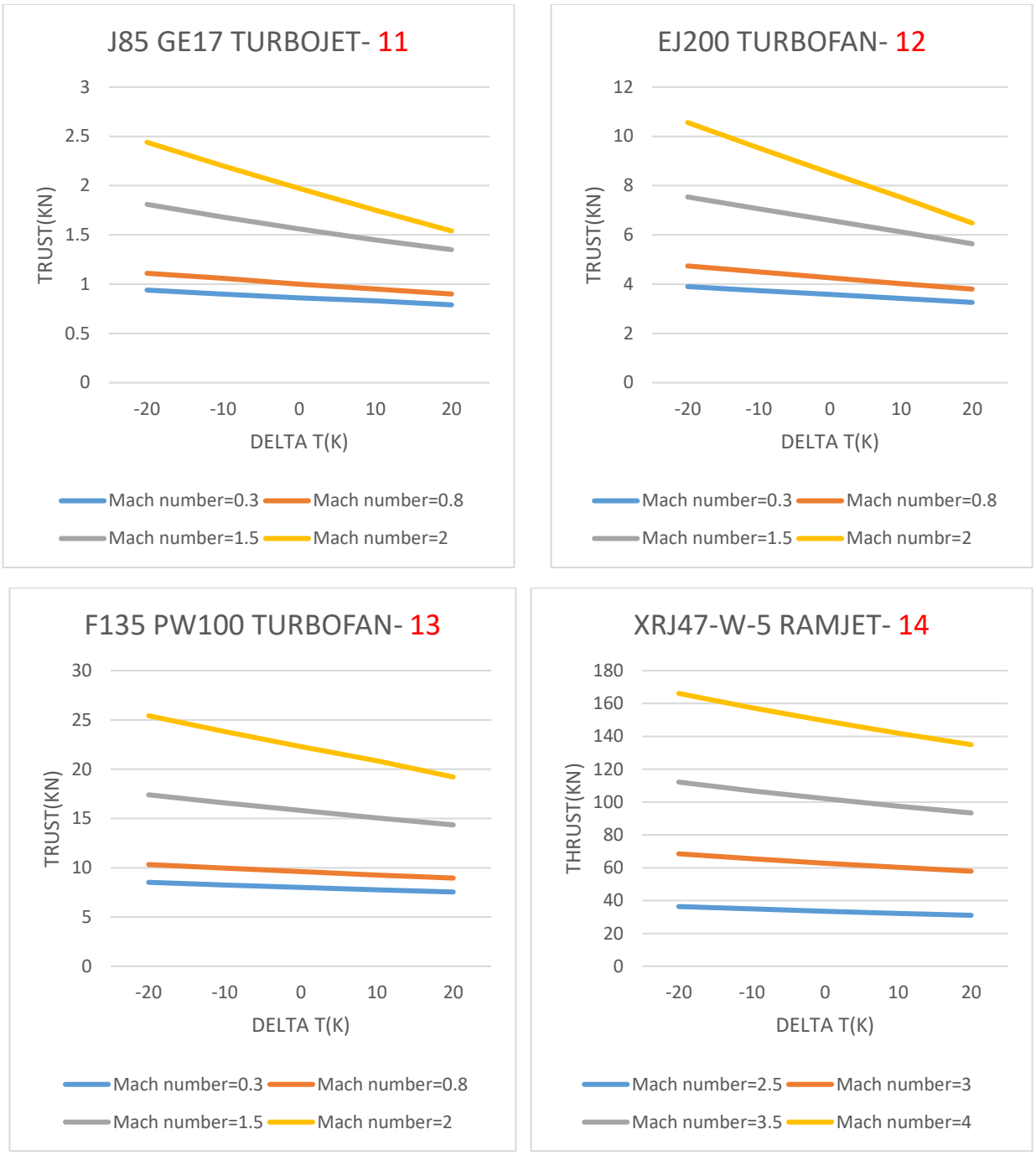

Fig. 12. Thrust changes for J85GE17 turbojet, F135 PW100 turbofan, EJ200 turbofan, XRJ47-W-5 ramjet engines at an altitude of 20,000 meters and for hydrogen fuel with changes in inlet air temperature.

Fuel flow rate changes for J85GE17 turbojet, F135 PW100 turbofan, EJ200 turbofan, XRJ47-W-5 ramjet engines at an altitude of 20,000 meters and for hydrogen fuel for J85GE17 turbojet, F135 PW100 turbofan, EJ200 turbofan, XRJ47-W-5 ramjet engines. It is shown in Fig. 13 with the changes of the inlet air temperature. Since the actual flow rate of the inlet air increases with the decrease of the inlet air temperature, more thermal energy is needed to bring the flow temperature to the burner outlet temperature. Therefore, as the temperature of the intake air decreases, the fuel flow rate increases.

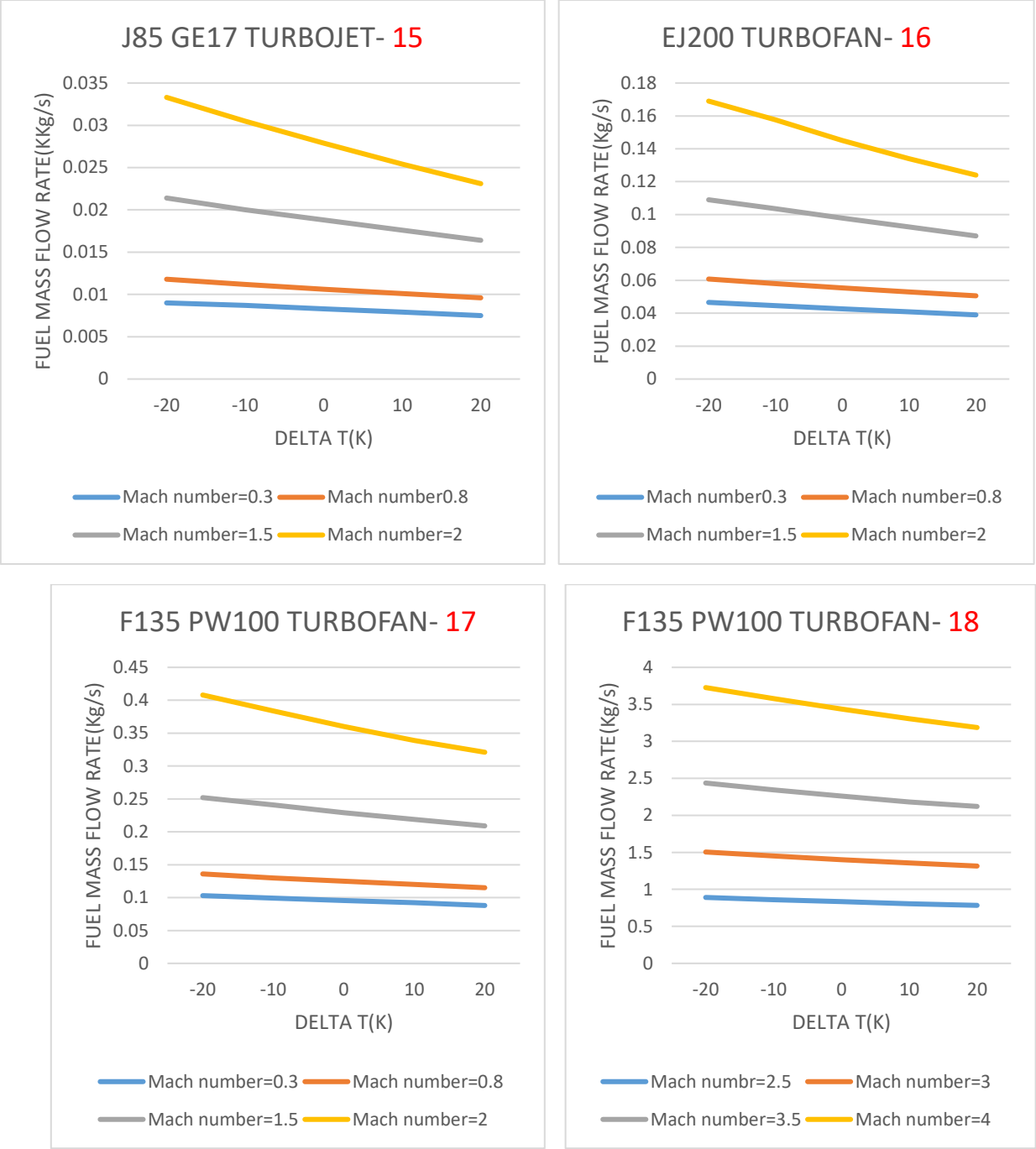

Fig. 13. changes in fuel consumption for J85GE17 turbojet, F135 PW100 turbofan, EJ200 turbofan, XRJ47-W-5 ramjet engines at an altitude of 20,000 meters and for hydrogen fuel with changes in inlet air temperature.

TSFC changes for J85GE17 turbojet, F135 PW100 turbofan, EJ200 turbofan, XRJ47-W-5 ramjet engines at an altitude of 20,000 meters and for hydrogen fuel with changes in inlet air temperature are shown in Figure 14. For J85GE17 turbojet.

F135PW100 turbofan, EJ200 turbofan, XRJ47-W-5 ramjet Since the increase in thrust force due to the decrease in intake air temperature is greater than the increase in fuel consumption due to the decrease in intake air temperature, therefore TSFC decreases with the decrease in intake air temperature.

Fig. 14. TSFC changes for J85GE17 turbojet, F135 PW100 turbofan, EJ200 turbofan, XRJ47-W-5 ramjet engines at an altitude of 20,000 meters and for hydrogen fuel with changes in inlet air temperature.

Thermal efficiency changes for J85GE17 turbojet engines, F135 PW100 turbofan, EJ200 turbofan, at an altitude of 20,000 meters and for hydrogen fuel with changes in inlet air temperature are shown in Figure 15. For J85GE17 turbojet engines, F135 PW100 turbofan, EJ200 turbofan, with a decrease in the temperature of the inlet air, the increase in the air flow rate (real inlet air mass flow rate) is greater than the increase in the fuel mass flow rate (fuel mass flow rate), so the changes in the kinetic energy of the

flow along the engine with the rate The magnitude increases as the heating rate increases. So, the thermal efficiency of the cycle increases with the decrease of inlet air temperature drop.

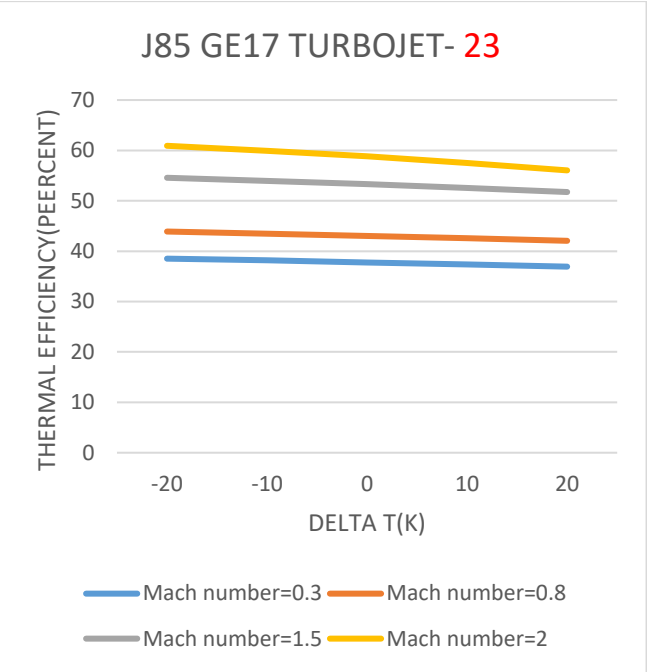

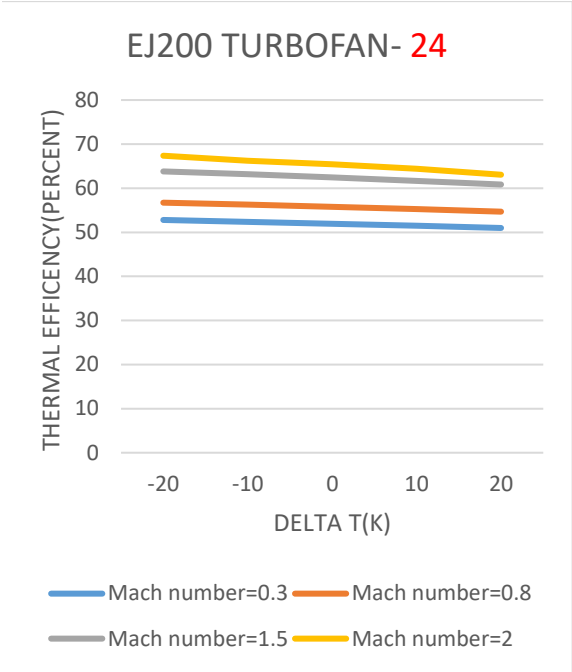

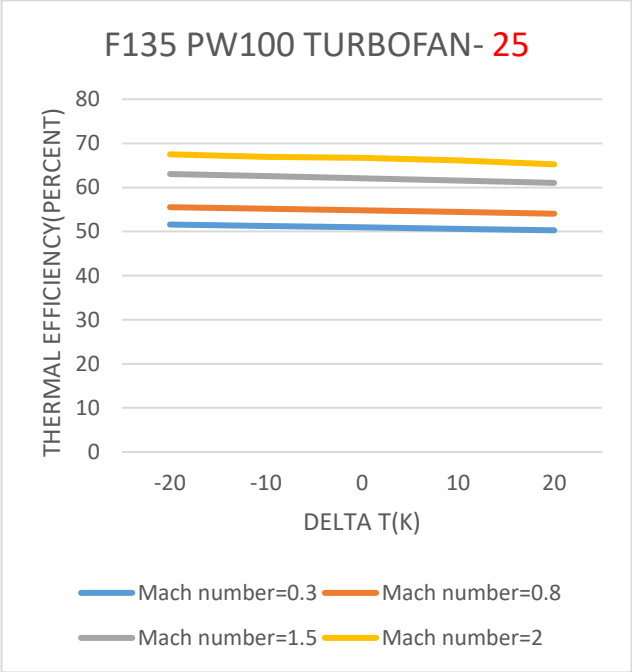

Fig. 15. changes in thermal efficiency for J85GE17 turbojet engines, F135 PW100 turbofan, EJ200 turbofan, at an altitude of 20,000 meters and for hydrogen fuel with changes in inlet air temperature.

Propulsion efficiency changes for J85GE17 turbojet engines, F135 PW100 turbofan, EJ200 turbofan, XRJ47-W-5 ramjet at an altitude of 20000 meters and for hydrogen fuel with changes in inlet air temperature are shown in Figure 16. For J85GE17 turbojet engines F135 PW100 turbofan, EJ200 turbofan, XRJ47-W-5 ramjet, as the temperature of the inlet air decreases, the propulsion efficiency

decreases because the rate of increase in the thrust product in the cruising speed due to the decrease in the temperature of the inlet air is greater than the rate of increase in the kinetic energy of the flow along the engine.

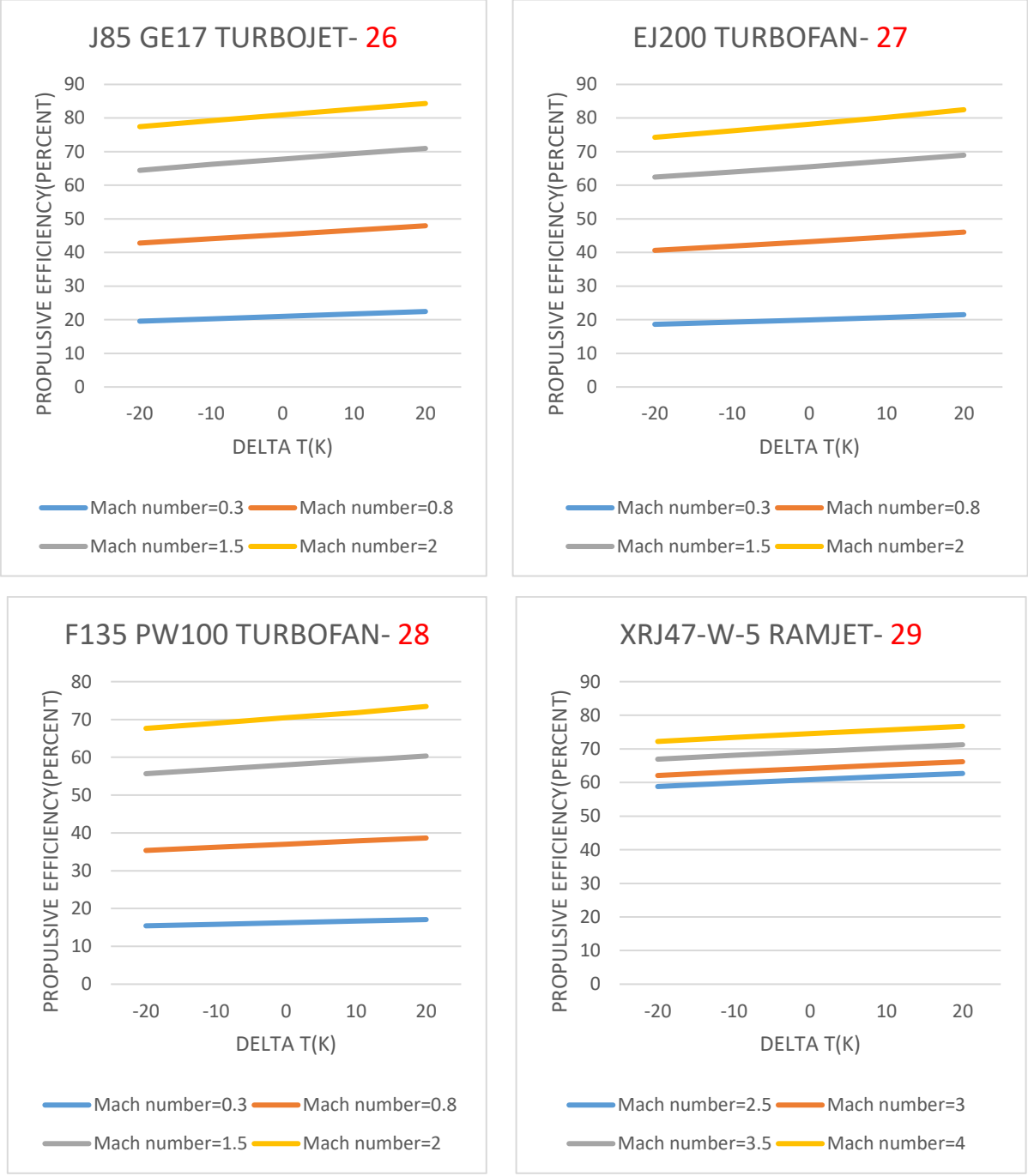

Fig. 16. Propulsion efficiency changes for J85GE17 turbojet, F135 PW100 turbofan, EJ200 turbofan, XRJ47-W-5 ramjet engines at an altitude of 20,000 meters and for hydrogen fuel with changes in inlet air temperature.

Changes in the emission intensity of nitrogen oxides (EINOx) for J85GE17 turbojet engines, F135 PW100 turbofan, EJ200 turbofan, at an altitude of 20,000 meters and for hydrogen fuel with changes in

inlet air temperature are shown in Figure 17 for J85GE17 engines. turbojet. F135 PW100 turbofan, EJ200 turbofan, by reducing the inlet air temperature EINOx is reduced.

Fig. 17. changes in nitrogen oxide emission intensity (EINOx) for J85G17 turbojet engines, F135 PW100 turbofan, EJ200 turbofan, at an altitude of 20,000 meters and for hydrogen fuel with changes in inlet air temperature.

Intensity of influence of inlet air temperature on the performance of F135 PW100 turbofan, EJ200 turbofan, XRJ47-W-5 ramjet engines in this study, we have investigated the severity of the influence of inlet air temperature deviations on TSF and TSFC for XRJ47-W-5 ramjet engine, as well as EINOx and TSF deviations for F135 PW100 turbofan, EJ200 turbofan engines with Mach deviations. Comparisons of the desired parameters have been made in the two cases of $\Delta T=+10$ and $\Delta T=-10$ degrees Kelvin for

different flight Mach at a flight altitude of 20,000 meters for hydrogen fuel. For the EJ200 turbofan engine, the percentage of TSF parameter deviations in ΔT=+10 and ΔT=-10 degrees Kelvin for different flight Mach number at a flight altitude of 20,000 meters for hydrogen fuel at flight Mach numbers of 0.3, 0.8, 1.5, and 2 respectively +4.41 and +6.57 and +10.06% and +20.86%. Also, the percentage of EI-NOx parameter deviations in the two conditions of ΔT=+10 and ΔT=-10 degrees Kelvin for different flight Mach numbers at a flight altitude of 20,000 meters for hydrogen fuel at flight Mach numbers of 0.3, 0.8, and 1 5 and 2 are -0.02, -25.98, -30.37 and -34.71%, respectively. For the F135 PW100 turbofan engine, the percentage of TSF parameter deviations in the two conditions of ΔT=+10 and ΔT=-10 degrees Kelvin for different flight Mach numbers at a flight altitude of 20,000 meters to per hydrogen fuel at Mach 0.3, 0.8, 1.5, and 2 are +1.49, +2.57, +5.16, and +9.05%, respectively. Also, the percentage of EINOx parameter deviations in the two cases ΔT=+10 and ΔT=-10 degrees Kelvin per Different cruising Mach numbers at the cruising altitude of 20,000 meters for hydrogen fuel at cruising Mach numbers of 0.3, 0.8, 1.5, and 2 are -24.26, -26.36, -30.93, and -35.24%, respectively. Therefore, for F135 PW100, EJ200 turbofan engines, at a constant altitude, with an increase in the Mach number, the TSF increases with a larger pitch for a decrease in the inlet air temperature. Also, at a constant altitude, with an increase in the Mach number, the clearance for a decrease in the inlet air temperature EINOx increases with a pitch. The larger it is, the smaller it is. For the XRJ47-W-5 ramjet engine, the percentage of TSF parameter deviations in ΔT=+10 and ΔT=-10 degrees Kelvin for different cruising Mach numbers at cruising altitude of 20,000 meters for hydrogen fuel at cruising Mach numbers of 2.5, 3, 3.5, and 4 respectively + 3.54, +4.31, +5.53, and +7.39%. Also, the percentage of TSFC parameter deviations in TΔ=+10 and TΔ=-10 degrees Kelvin for different cruising Mach numbers at a cruising altitude of 20,000 meters for hydrogen fuel at cruising Mach numbers of 2.5 and 3 And 3.5 and 4 are -1.51, -1.62, -1.96 and -2.49%, respectively. Therefore, for the XRJ47-W-5 ramjet engine, at a constant altitude, with an increase in the Mach number, the TSF increases with a larger pitch for a decrease in the inlet air temperature. Also, at a constant height, with an increase in the Mach number, the clearance for a decrease in the inlet air temperature, TSFC, increases with a larger pitch. Decreases.

4.3. OPTIMIZATION

In this study, optimization for hydrogen fuel has been performed for three separate objective functions:

- Maximizing Thrust-to-Weight Ratio (TSF)
- Minimizing Thrust-Specific Fuel Consumption (TSFC)
- Maximizing Thermal Efficiency

The optimization is conducted in two distinct phases:

Phase I: In this phase of optimization, the altitude range of 20,000 meters to 30,000 meters and the Mach range of 2 to 3 for J85GE17 turbojet, F135 PW100 turbofan, and EJ200 turbofan engines, as well as the Mach range of 3 to 4.5 for XRJ47-W-5 ramjet engine, have been considered.

Optimization has been carried out to determine the optimal parameters under these conditions for each of the engines.

The optimized parameters for J85GE17 turbojet, F135 PW100 turbofan, EJ200 turbofan, and XRJ47-W-5 ramjet engines in Phase I are summarized in Table 6. This table presents the optimized parameters for the J85GE17 turbojet, F135 PW100 turbofan, EJ200 turbofan, and XRJ47-W-5 ramjet engines under Phase I conditions, encompassing an altitude range of 20,000 meters to 30,000 meters and Mach ranges of 2 to 3 for turbojets and turbofans, and 3 to 4.5 for the ramjet engine. These optimized parameters reflect the

outcomes of the optimization process aimed at maximizing thrust-to-weight ratio (TSF), minimizing thrust-specific fuel consumption (TSFC), and maximizing thermal efficiency.

Table 6 demonstrates the optimal parameter values obtained through the optimization process for various engines including J85GE17 turbojet, F135 PW100 turbofan, EJ200 turbofan, and XRJ47-W-5 ramjet, under the specified PHASE 1 conditions.

Table 6. Optimized Parameters for Hydrogen Fuel Engines in Phase I

Parameters	Limits	XRJ47-W-5 ramjet	F135 PW100 turbofan	EJ200 turbofan	J85 GE 17 TURBOJET
Burner inlet temperature(k)	Upper	2400	2200	2150	2000
	Lower	2000	1000	1000	1000
Compressor pressure ratio	Upper	-	30	30	15
	Lower	-	2	2	2
ΔT(k)	Upper	20	20	20	20
	Lower	-20	-20	-20	-20
Flight altitude(m)	Upper	30000	30000	30000	30000
	Lower	20000	20000	20000	20000
Flight Mach number	Upper	4.5	3	3	3
	Lower	3	2	2	2
Fan pressure ratio	Upper	-	6	6	-
	Lower	-	2	2	-
Design bypass ratio	Upper	-	10	10	-
	Lower	-	0.1	0.1	-

Table 7 presents the optimization constraints applied to J85GE21 turbojet, F135 PW100 turbofan, EJ200 turbofan, and XRJ47-W-5 ramjet engines within the context of PHASE 1 conditions.

Table 7. Optimization constraints applied to J85GE21 turbojet, F135 PW100 turbofan, EJ200 turbofan, and XRJ47-W-5 ramjet engines within the context of PHASE 1 conditions.

Objective function	***Parameters***	***Limits***	***XRJ47-W-5 ramjet***	***F135 PW100 turbofan***	***EJ200 turbofan***	***J85 GE 17 TURBOJET***
TSF	Thrust (KN)	Upper	50	45	25	10
		Lower	6	22.29	10.04	1.96
	TSFC(g/KNs)	Upper	25	17	15	15
		Lower	5	4	4	5
TSFC	Fuel mass flow rate (Kg/s)	Upper	0.850	0.370	0.160	0.030
		Lower	0.002	0.100	0.050	0.002
	TSF(Ns/Kg)	Upper	1500	700	500	500
		Lower	990	500	380	273
Thermal efficiency	TSF(Ns/Kg)	Upper	-	800	500	500
		Lower	-	495	385	450
	TSFC(g/KNs)	Upper	-	17	16	16
		Lower	-	4	2	5

Table 8. observes the parameter values that have been optimized for J85GE21 turbojet, F135 PW100 turbofan, EJ200 turbofan, and XRJ47-W-5 ramjet engines to maximize the Total Specific Force (TSF) under the defined PHASE 1 conditions.

Table 8. Optimized parameter values for J85GE21 turbojet, F135 PW100 turbofan, EJ200 turbofan, and XRJ47-W-5 ramjet engines to maximize the Total Specific Force (TSF) under the defined PHASE 1 conditions.

Parameters	***XRJ47-W-5 ramjet***	***F135 PW100 turbofan***	***EJ200 turbofan***	***J85 GE 17 TURBOJET***
Burner exit temperature(K)	2399	2122.71	1841	1595.31
Overall compressor pressure ratio	-	28.328	29.613	14.553
Fan pressure ratio	-	5.704	5.440	-
ΔT(K)	-19.94	-19.98	-19.54	-19.97
Design bypass ratio	-	0.102	0.102	-
Flight altitude (m)	21253	20749	21038.2	21597.6
Flight Mach number	3	2.01	2	2

Table 9 provides the optimized parameter values for J85GE17 turbojet, F135 PW100 turbofan, EJ200 turbofan, and XRJ47-W-5 ramjet engines, aiming to minimize the Total Specific Fuel Consumption (TSFC) in compliance with PHASE 1 conditions.

Table 9. optimized parameter values for J85GE17 turbojet, F135 PW100 turbofan, EJ200 turbofan, and XRJ47-W-5 ramjet engines, aiming to minimize the Total Specific Fuel Consumption (TSFC) in compliance with PHASE 1 conditions

Parameters	**XRJ47-W-5 ramjet**	**F135 PW100 turbofan**	**EJ200 turbofan**	**J85 GE 17 TURBOJET**
Burner exit temperature(K)	2157.99	1775.46	1558.93	1196.3
Overall compressor pressure ratio	-	26.187	28.572	14.996
Fan pressure ratio	-	4.162	4.730	-
ΔT(K)	-19.99	-19.94	-19.78	-19.56
Design bypass ratio	-	0.130	0.114	-
Flight altitude (m)	22810.8	23308.5	21946	24718
Flight Mach number	3.05	2	2	2

Table 10 showcases the optimized parameter values for J85GE17 turbojet, F135 PW100 turbofan, EJ200 turbofan, and XRJ47-W-5 ramjet engines, with the objective of maximizing thermal efficiency within the PHASE 1 conditions.

Table 10. Optimized parameter values for J85GE17 turbojet, F135 PW100 turbofan, EJ200 turbofan, and XRJ47-W-5 ramjet engines, with the objective of maximizing thermal efficiency within the PHASE 1 conditions.

Burner exit temperature(K)	2147.99	2149.99	1511.91
Overall compressor pressure ratio	29.941	29.948	14.998
Fan pressure ratio	5.951	5.700	-

ΔT (K)	-19.97	-19.98	-19.99
Design bypass ratio	0.419	0.939	-
Flight altitude (m)	20010.4	20008.2	21768
Flight Mach number	2.240	2.241	2.084

- *the optimized performance outcomes*
  - ❖ J85 GE17 turbojet

Table 11 demonstrating the performance outcomes of the optimized J85GE17 turbojet cycle, this table illustrates the effects of various objective functions within the PHASE 1 conditions using hydrogen fuel.

Table 11. the performance outcomes of the optimized J85GE17 turbojet cycle, this table illustrates the effects of various objective functions within the PHASE 1 conditions using hydrogen fuel.

Objective function	Thrust (KN)	TSF(Ns/Kg)	Fuel mass flow rate (Kg/s)	TSFC	Propulsion efficiency (%)	Thermal efficiency (%)
TSF	3.12	531	0.046	14.997	67.85	67.64
TSFC	0.98	273.240	0.0137	13.173	80.15	68.35
Thermal efficiency	2.88	432.55	0.042	14.848	72.11	68.05

  - ❖ EJ200 turbofan

Table 12 is highlighting the performance results of the optimized EJ200 turbofan cycle, this table provides insight into the impact of different objective functions within the PHASE 1 conditions using hydrogen fuel.

Table 12. the performance results of the optimized EJ200 turbofan cycle, this table provides insight into the impact of different objective functions within the PHASE 1 conditions using hydrogen fuel.

Objective function	Thrust (KN)	TSF(Ns/Kg)	Fuel mass flow rate (Kg/s)	TSFC	Propulsion efficiency (%)	Thermal efficiency (%)
TSF	12.40	543.263	0.186	14.994	67.62	67.82
TSFC	7.53	376.933	0.102	13.637	74.78	63.74
Thermal efficiency	13.98	386.87	0.223	15.991	76.70	70.88

  - ❖ F135 PW100 turbofan

Table 13 explores the performance outcomes of the optimized F135 PW100 turbofan cycle, shedding light on the influence of different objective functions within the PHASE 1 conditions using hydrogen fuel.

Table 13. the performance outcomes of the optimized F135 PW100 turbofan cycle, shedding light on the influence of different objective functions within the PHASE 1 conditions using hydrogen fuel.

Objective function	Thrust (KN)	TSF(Ns/Kg)	Fuel mass flow rate (Kg/s)	TSFC	Propulsion efficiency (%)	Thermal efficiency (%)
TSF	28.66	690.219	0.487	16.998	62.29	67.53
TSFC	13.87	500.216	0.208	15.037	69.37	65.75
Thermal efficiency	31.06	495.849	0.223	16.998	71.99	69.82

- ❖ XRJ47-W-5 ramjet

Table 14 is illustrating the performance outcomes of the optimized XRJ47-W-5 ramjet cycle, this table offers an understanding of the consequences of different objective functions within the PHASE 1 conditions using hydrogen fuel.

Table 14. the performance outcomes of the optimized XRJ47-W-5 ramjet cycle, this table offers an understanding of the consequences of different objective functions within the PHASE 1 conditions using hydrogen fuel.

Objective function	Thrust (KN)	TSF(Ns/Kg)	Fuel mass flow rate (Kg/s)	TSFC	Propulsion efficiency (%)
TSF	60	1138.446	1.387	23.113	60.86
TSFC	40.49	990.045	0.847	20.926	63.91

PHASE II: In this phase of optimization, the engines including J85GE21 turbojet, F135 PW100 turbofan, EJ200 turbofan, and XRJ47-W-5 ramjet have been subjected to optimization within the altitude range of 30000 meters to 40000 meters and Mach range of 2.5 to 3. Table 15 displays the optimal parameter values obtained through the optimization process for J85GE21 turbojet, F135 PW100 turbofan, EJ200 turbofan, and XRJ47-W-5 ramjet engines under the specified PHASE 2 conditions.

Table 15 displays the optimal parameter values obtained through the optimization process for J85GE21 turbojet, F135 PW100 turbofan, EJ200 turbofan, and XRJ47-W-5 ramjet engines under the specified PHASE 2 conditions.

Table 15. the optimized parameter values for J85GE21 turbojet, F135 PW100 turbofan, EJ200 turbofan, and XRJ47-W-5 ramjet engines within the context of PHASE 2 conditions.

Objective function	Parameters	Limits	XRJ47-W-5 ramjet	F135 PW100 turbofan	EJ200 turbofan	J85 GE 21 TURBOJET
TSF	Thrust (KN)	Upper	30	20	10	5
		Lower	18	4.85	1.38	0.22
	TSFC(g/KNs)	Upper	25	26	28	30
		Lower	5	4	5	5
TSFC	Fuel mass flow rate (Kg/s)	Upper	0.500	0.125	0.040	0.007
		Lower	0.050	0.001	0.001	0.002
	TSF(Ns/Kg)	Upper	1000	600	500	500
		Lower	930	296	146	75
Thermal efficiency	TSF(Ns/Kg)	Upper	-	600	500	150
		Lower	-	295	150	55
	TSFC(g/KNs)	Upper	-	24	26	34
		Lower	-	5	5	5

Table 16 illustrates the optimization constraints applied to J85GE21 turbojet, F135 PW100 turbofan, EJ200 turbofan, and XRJ47-W-5 ramjet engines within the context of PHASE 2 conditions.

Table 16. the optimization constraints applied to J85GE21 turbojet, F135 PW100 turbofan, EJ200 turbofan, and XRJ47-W-5 ramjet engines within the context of PHASE 2 conditions.

Objective function	***Parameters***	***Limits***	***XRJ47-W-5 ramjet***	***F135 PW100 turbofan***	***EJ200 turbofan***	***J85 GE 21 TURBOJET***
TSF	Thrust (KN)	Upper	30	20	10	5
		Lower	18	4.85	1.38	0.22
	TSFC(g/KNs)	Upper	25	26	28	30
		Lower	5	4	5	5
TSFC	Fuel mass flow rate (Kg/s)	Upper	0.500	0.125	0.040	0.007
		Lower	0.050	0.001	0.001	0.002
	TSF(Ns/Kg)	Upper	1000	600	500	500
		Lower	930	296	146	75
Thermal efficiency	TSF(Ns/Kg)	Upper	-	600	500	150
		Lower	-	295	150	55
	TSFC(g/KNs)	Upper	-	24	26	34
		Lower	-	5	5	5

Table 17 presents the optimized parameter values for J85GE21 turbojet, F135 PW100 turbofan, EJ200 turbofan, and XRJ47-W-5 ramjet engines with the objective of maximizing the Total Specific Force (TSF), within the PHASE 2 conditions

Table 17. the optimized parameter values for J85GE21 turbojet, F135 PW100 turbofan, EJ200 turbofan, and XRJ47-W-5 ramjet engines with the objective of maximizing the Total Specific Force (TSF), within the PHASE 2 conditions

	XRJ47-W-5 ramjet	**F135 PW100 turbofan**	**EJ200 turbofan**	**J85 GE 21 TURBOJET**
Burner exit temperature (K)	2400	2199.97	2149.86	1999.97
Overall compressor pressure ratio	-	2.026	2.091	2
Fan pressure ratio	-	5.682	3.983	-
ΔT (K)	-19.96	-19.62	-19.58	-19.97
Design bypass ratio	-	0.100	0.100	-
Flight altitude (m)	30006	30023.5	30016.6	30025
Flight Mach number	3.500	2.501	2.500	2.504

In accordance with the PHASE 2 conditions, Table 18 demonstrates the optimized parameter values for J85GE21 turbojet, F135 PW100 turbofan, EJ200 turbofan, and XRJ47-W-5 ramjet engines aiming to minimize the Total Specific Fuel Consumption (TSFC).

Table 18. the optimized parameter values for J85GE21 turbojet, F135 PW100 turbofan, EJ200 turbofan, and XRJ47-W-5 ramjet engines aiming to minimize the Total Specific Fuel Consumption (TSFC)- Phase 2

	XRJ47-W-5 ramjet	***F135 PW100 turbofan***	***EJ200 turbofan***	***J85 GE 21 TURBOJET***
Burner exit temperature(K)	2222.19	1789.75	1709.48	1611.93
Overall compressor pressure ratio	-	17.773	14.912	11.183
Fan pressure ratio	-	5.687	4.922	-
ΔT(K)	-19.98	-19.98	-19.99	-19.78
Design bypass ratio	-	0.100	0.108	-
Flight altitude(m)	30001.1	30009.3	32173.4	35774.3
Flight Mach number	3.500	2.503	2.500	2.500

Highlighting the PHASE 2 conditions, Table 19 showcases the optimized parameter values for J85GE21 turbojet, F135 PW100 turbofan, EJ200 turbofan, and XRJ47-W-5 ramjet engines with the goal of maximizing thermal efficiency.

Table 19. the optimized parameter values for J85GE21 turbojet, F135 PW100 turbofan, EJ200 turbofan, and XRJ47-W-5 ramjet engines with the goal of maximizing thermal efficiency-Phase 2

	F135 PW100 turbofan	**EJ200 turbofan**	**J85 GE 21 TURBOJET**
Burner exit temperature(K)	2167.90	2147.18	1997.49
Overall compressor pressure ratio	11.291	9.827	10.075
Fan pressure ratio	5.910	4.143	-
ΔT(K)	-19.97	-19.99	-19.99
Design bypass ratio	0.175	0.100	-
Flight altitude(m)	30005.3	30002	30000.7
Flight Mach number	2.911	2.999	2.998

Performance of Optimized Cycles in PHASE2:

The outcomes of optimized cycles based on J85GE21 turbojet, F135 PW100 turbofan, EJ200 turbofan, and XRJ47-W-5 ramjet engines using various objective functions within PHASE 2 conditions are investigated.

A) J85 GE17 turbojet:

Table 20 illustrates the performance results of the optimized J85 GE17 turbojet cycle under various objective functions within the PHASE 2 conditions using hydrogen fuel.

Table 20. the optimized J85 GE17 turbojet cycle under various objective functions within the PHASE 2 conditions using hydrogen fuel.

Objective function	Thrust (KN)	TSF(Ns/Kg)	Fuel mass flow rate (Kg/s)	TSFC	Propulsion efficiency (%)	Thermal efficiency (%)
TSF	1.99	677.220	0.045	22.631	68.54	58.25
TSFC	0.35	292.860	0.0069	6.645	83.66	68.32
Thermal efficiency	2.22	389.690	0.054	24.496	81.77	74.33

B) EJ200 turbofan:

By showcasing the performance outcomes of the optimized EJ200 turbofan cycle, Table 21 provides insights into the impact of different objective functions within the PHASE 2 conditions using hydrogen fuel.

Table 21. the performance outcomes of the optimized EJ200 turbofan cycle within the PHASE 2 conditions using hydrogen fuel for impact of different objective functions

Objective function	Thrust (KN)	TSF(Ns/Kg)	Fuel mass flow rate (Kg/s)	TSFC	Propulsion efficiency (%)	Thermal efficiency (%)
TSF	6.48	659.139	0.154	23.858	69.41	54.13
TSFC	2.05	292.689	0.040	19.505	83.58	60.41
Thermal efficiency	7.38	415.143	0.184	24.995	69.70	69.70

C) F135 PW100 turbofan:

Table 22 explores the performance results of the optimized F135 PW100 turbofan cycle, shedding light on the influence of different objective functions within the PHASE 2 conditions using hydrogen fuel.

Table 22. the performance results of the optimized F135 PW100 turbofan cycle, shedding light on the influence of different objective functions within the PHASE 2 conditions using hydrogen fuel.

Objective function	Thrust (KN)	TSF(Ns/Kg)	Fuel mass flow rate (Kg/s)	TSFC	Propulsion efficiency (%)	Thermal efficiency (%)
TSF	11.54	676.356	0.284	24.607	68.89	51.95
TSFC	5.74	335.829	0.109	19.047	81.39	63.77
Thermal efficiency	11.50	412.926	0.276	24.048	80.72	68.48

D) XRJ47-W-5 ramjet:

Illustrating the performance outcomes of the optimized XRJ47-W-5 ramjet cycle, Table 23 offers an understanding of the consequences of different objective functions within the PHASE 2 conditions using hydrogen fuel.

Table 23. the consequences of the performance outcomes of the optimized XRJ47-W-5 ramjet cycle for different objective functions within the PHASE 2 conditions using hydrogen fuel.

Objective function	Thrust (KN)	TSF(Ns/Kg)	Fuel mass flow rate (Kg/s)	TSFC	Propulsion efficiency (%)
TSF	23.17	1048.770	0.551	23.8787	67.17
TSFC	20.56	930.218	0.448	21.826	69.62

5. Analysis of Optimization Results

Among the optimized cycles in PHASE 1 and PHASE 2, the highest propulsion efficiency at design point conditions belongs to the optimized cycle based on J85 GE17 turbojet with a focus on minimizing TSFC in PHASE 2. Additionally, the maximum TSF and minimum TSFC at design point conditions are achieved by the optimized cycles based on XRJ47-W-5 ramjet with a focus on maximizing TSF in PHASE 1, and the optimized cycle based on J85E17 with a focus on minimizing TSFC in PHASE 2.

Cycles Selection :

In this study, among the optimized cycles based on J85GE21 turbojet, F135 PW100 turbofan, and EJ200 turbofan engines in PHASE I and PHASE II using hydrogen fuel, one cycle was selected for each approach in each phase.

The selection criteria for the optimized cycles in PHASE I and 2 are respectively Thermal Efficiency (percent), $TPDP$ (KN/pa), Propulsive Efficiency (%), TSFC (g/KNs), and TSF (Ns/Kg). For both phases, cycle selection was performed based on two approaches: Energy Consumption and Environmental, as well as Power and Maneuverability.

Weighting coefficients for the Energy Consumption and Environmental, and Power and Maneuverability approaches are provided in Table 24.

Table 24. Weighting Coefficients for Energy Consumption and Environmental, and Power and Maneuverability Approaches

	TSF	**TSFC**	**Propulsive efficiency**	**TPDP**	**Thermal efficiency**	**EINOx**
Energy consumption and environmental	0	-0.85	0	0	+0.95	-0.90
Power and maneuver ability	+0.90	0	+0.85	+0.95	0	0

Therefore, in PHASE 1, considering the Energy Consumption and Environmental approach, the optimized cycle based on J85GE17 with a maximized TSF achieved the highest score, while the optimized cycle based on EJ200 with a maximized Thermal Efficiency obtained the lowest score. Hence, the optimized cycle based on J85GE17 with a maximized TSF and the Energy Consumption and Environmental approach was selected for PHASE 1.

Additionally, in PHASE 1, considering the Power and Maneuverability approach, the optimized cycle based on F135PW100 with a maximized TSF earned the highest score, while the optimized cycle based on J85GE17 with minimized TSFC obtained the lowest score. Thus, the optimized cycle based on F135PW100 with a maximized TSF and the Power and Maneuverability approach was chosen.

The Temperature-Entropy diagram for the optimized cycle based on J85GE17 with a maximized TSF and the optimized cycle based on F135PW100 with a maximized TSF at the design point conditions are illustrated in Figures 19 and 20, respectively.

The scores obtained by the optimized cycles in PHASE1 for the Energy consumption and environmental and Power and maneuver ability approaches are shown in Fig.18.

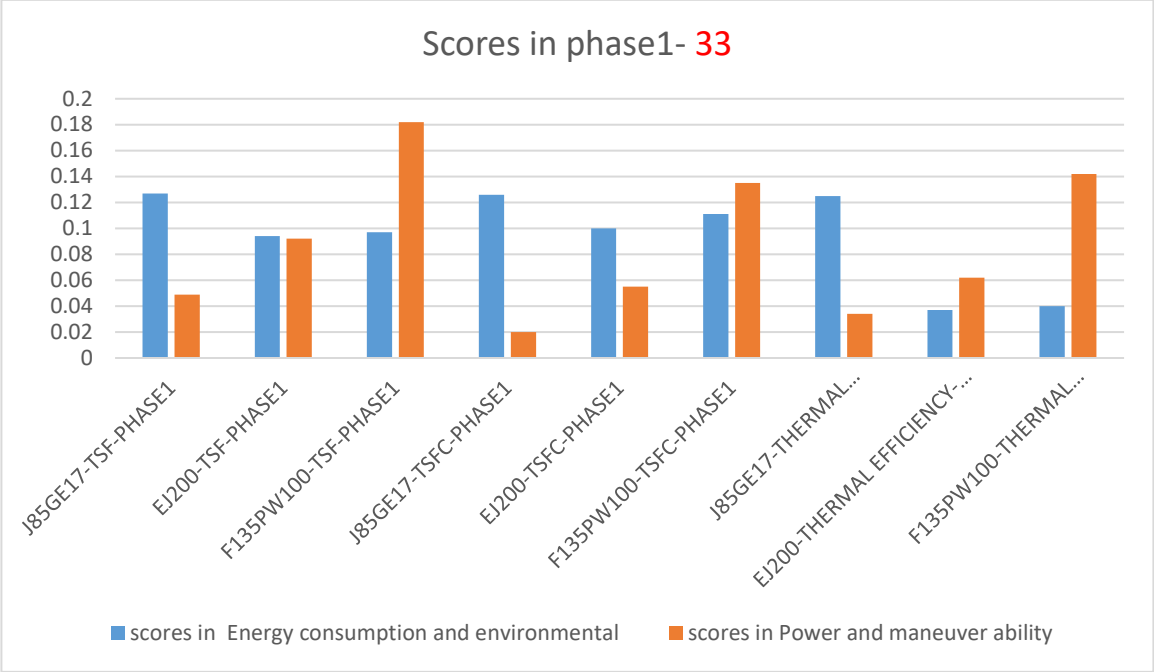

Fig. 18. Achieved Scores by Optimized Cycles in PHASE 1 for Energy Consumption and Environmental, and Power and Maneuverability Approaches.

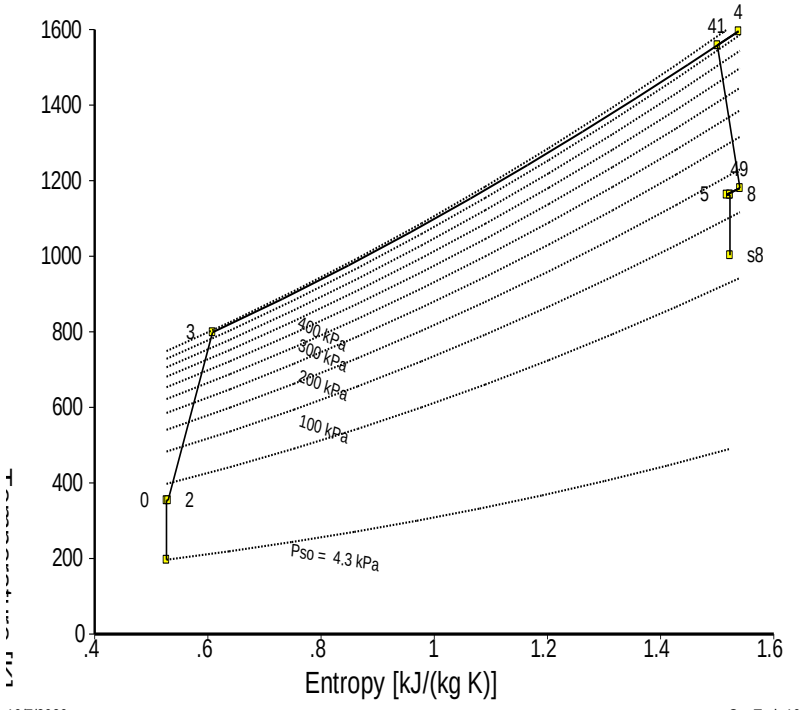

Fig. 19. Temperature-Entropy Diagram of the Optimized Cycle based on J85GE17 with Maximized TSF at Design Point Conditions

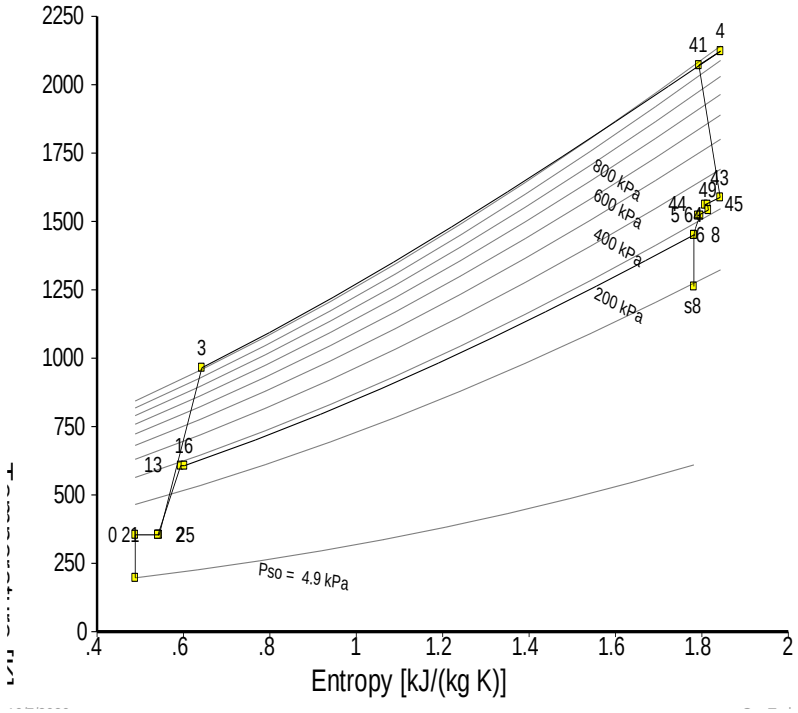

Fig. 20. Temperature-Entropy Diagram of the Optimized Cycle based on F135PW100 with Maximized TSF at Design Point Conditions.

The scores obtained by the optimized cycles in PHASE2 for the Energy consumption and environmental and Power and maneuver ability approaches are shown in Fig. 21.

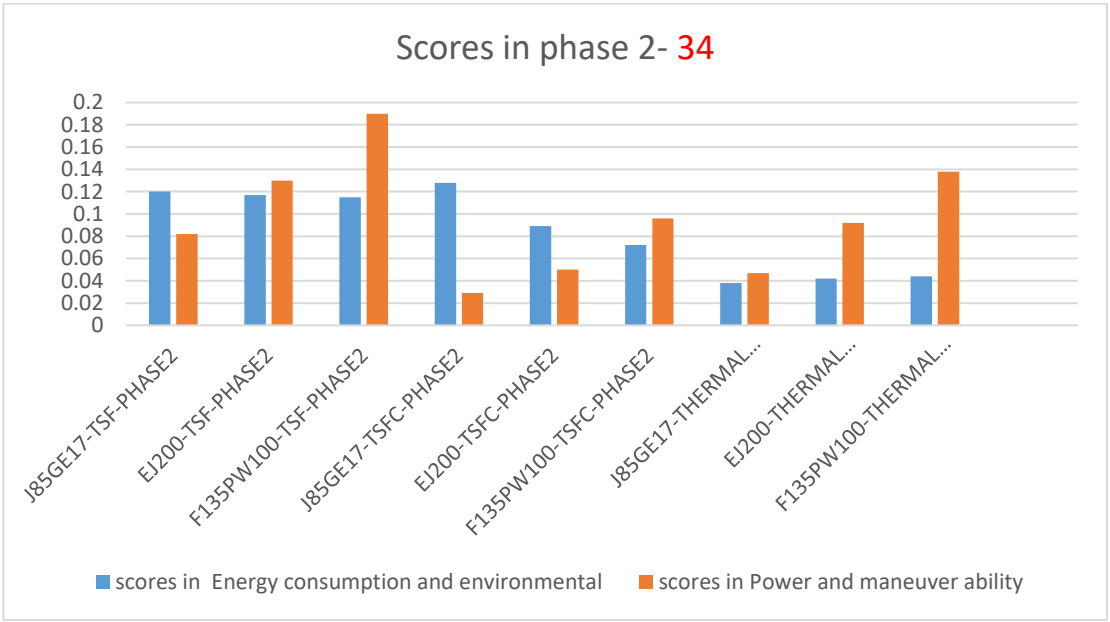

Fig. 21. Scores achieved by optimized cycles in PHASE 2 for Energy consumption and environmental and Power and maneuver ability approaches

Therefore, in PHASE 2, with the Energy consumption and environmental approach, the optimized cycle based on J85GE17 with minimized TSFC has achieved the highest score, and the optimized cycle based on J85GE17 with maximized Thermal efficiency has obtained the lowest score. Hence, the optimized cycle based on J85GE17 with minimized TSFC in PHASE 2 and with the Energy consumption and environmental approach has been selected. Additionally, in PHASE 2 with the Power and maneuver ability approach, the optimized cycle based on F135PW100 with maximized TSF has achieved the highest score, and the optimized cycle based on J85GE17 with minimized TSFC has obtained the lowest score. Therefore, the optimized cycle based on F135PW100 with maximized TSF in PHASE 2 and with the Power and maneuver ability approach has been chosen.

The Temperature-Entropy Diagram of the optimized cycle based on J85GE17 with minimized TSFC and the optimized cycle based on F135PW100 with maximized TSF at design point conditions are shown in Figures 22 and 23, respectively.

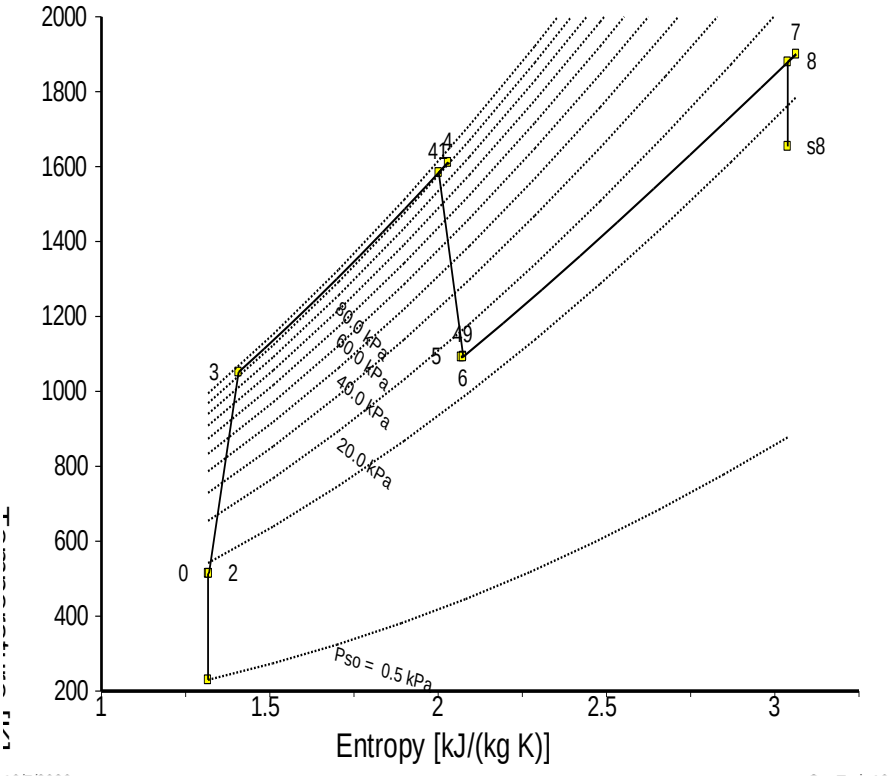

Fig. 22. Entropy-temperature diagram of the optimized cycle based on J85GE17 for minimizing TSFC at design point condition

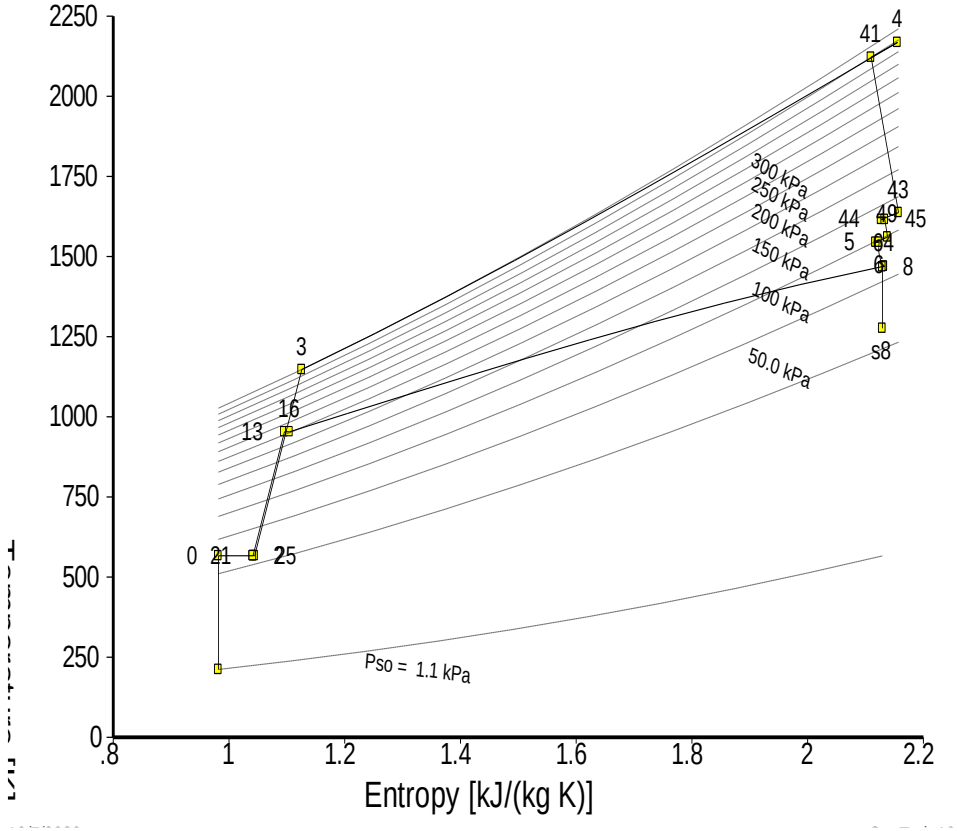

Fig. 23. Entropy-temperature diagram of the optimized cycle based on F135PW100 for maximizing TSF at design point conditions.

5.1. Comparison of Performance Parameters for Selected Cycles in Off-Design Conditions

Comparison of performance parameters for the selected cycles in PHASE 1 under off-design conditions (Ma=2.4 and H=27000m) for JP10 and Hydrogen fuels is presented in Table 25.

Table 25. Comparison of performance parameters for the selected cycles in PHASE 1 under off-design conditions (Ma=2.4 and H=27000m) for JP10 and Hydrogen fuels.

Cycle	Fuel type	TSF (Ns/Kg)	TSFC (g/KNs)	Fuel mass flow rate (Kg/s)	Thermal efficiency (%)	Propulsive efficiency (%)
F135 -TSF	Hydrogen	527.486	18.687	0.243	69.07	72.46
	JP10	491.889	52.342	0.636	65.374	74.57
J85 -TSF	Hydrogen	371.280	17.221	0.026	70.13	78.51
	JP10	354.570	48.904	0.072	67.05	79.80

Table 26 illustrates the comparison of performance parameters for the selected cycles in PHASE 2 under off-design conditions (Ma=3 and H=33000m) for JP10 and Hydrogen fuels.

Table 26. Comparison of Performance Parameters for Selected Cycles in PHASE 2 under Off-Design Conditions (Ma=3 and H=33000m) for JP10 and Hydrogen Fuels.

Cycle	Fuel type	TSF (Ns/Kg)	TSFC (g/KNs)	Fuel mass flow rate (Kg/s)	Thermal efficiency (%)	Propulsive efficiency (%)
F135 -TSF	Hydrogen	541.940	27.971	0.292	58.42	77.27
	JP10	501.528	78.863	0.763	54.92	79.75
J85 -TSFC	Hydrogen	124.560	32.994	0.014	68.19	93.20
	JP10	113.120	98.387	0.039	64.54	94.11

6. CONCLUSIONS

In the present study, the impact of altitude and flight Mach number on the performance parameters including thrust, specific fuel consumption (TSFC), fuel flow rate, and thermal efficiency of the XRJ47-W-5 ramjet, F135PW100 turbofan, EJ200 turbofan, and J85 GE17 turbojet engines has been investigated. The obtained results can be summarized as follows:

- For the F135PW100 turbofan, EJ200 turbofan, J85 GE17 turbojet, and XRJ47-W-5 ramjet engines, with an increase in flight Mach number, thrust, fuel flow rate, and thermal efficiency increase, while TSFC decreases.
- The study also examined the effect of variations in inlet air temperature on the performance parameters of the mentioned engines, including thrust, TSFC, fuel flow rate, thermal and propulsive efficiency, as well as nitrous oxide emissions (EINOx). Decreasing the inlet air temperature leads to an increase in thrust, TSFC, and fuel flow rate, while thermal efficiency and propulsive efficiency decrease. Additionally, EINOx decreases with decreased inlet air temperature for the mentioned engines.
- The study further investigated the impact of flight Mach number on the sensitivity of inlet air temperature variations on the performance of the engines. For the XRJ47-W-5 ramjet engine, increasing the flight Mach number intensifies the effect of variations in inlet air temperature, resulting in increased TSF and decreased TSFC due to the lowered inlet air temperature. Similarly, for the F135PW100 turbofan, EJ200 turbofan, and J85 GE17 turbojet engines, increasing flight Mach number intensifies the effect, leading to decreased EINOx and increased TSF due to the decreased inlet air temperature.
- The influence of different fuel types on thrust and TSFC of the engines was investigated. Increasing the fuel's heating value leads to a decrease in fuel flow rate and TSFC, while decreasing the fuel's molecular weight increases thrust. Therefore, among the studied fuels, hydrogen fuel yields the lowest TSFC and highest thrust.
- The optimal operating conditions were determined using the TOPSIS decision-making method in PHASE1 and PHASE 2 based on the Energy consumption and environmental approach. The results revealed that the optimized cycle based on the J85 GE17 engine, considering the maximization of TSF, and the optimized cycle based on the F135 PW100 engine, considering the maximization of thrust, achieved the best performance.

- The optimal operating conditions were also determined using the TOPSIS decision-making method in PHASE1 and PHASE 2 based on the Power and maneuverability approach. The results indicated that the optimized cycle based on the F135 PW100 engine, considering the maximization of TSF, achieved the best performance.

Conflicts of Interest:

The authors declare that there are no conflicts of interest regarding the publication of this paper.

Acknowledgments:

References

[1] Sabzehali M, Hossein Rabiee A, Alibeigi M, Mosavi A. Predicting the energy and exergy performance of F135 PW100 turbofan engine via deep learning approach. Energy Convers Manag 2022;265. https://doi.org/10.1016/j.enconman.2022.115775.

[2] Oates GC. Aerothermodynamics of gas turbine and rocket propulsion. Aiaa; 1997.

[3] Saravanamuttoo HIH, Rogers GFC, Cohen H. Gas turbine theory. Pearson education; 2001.

[4] Cumpsty N, Heyes A. Jet propulsion. Cambridge University Press; 2015.

[5] Farouk N, Sheng L, Hayat Q. Effect of ambient temperature on the performance of gas turbines power plant. Int J Comput Sci Issues 2013;10:439.

[6] Rahaman MM, Abdullah M, Rahman A. Measuring service quality using SERVQUAL model: A study on PCBs (Private Commercial Banks) in Bangladesh. Bus Manag Dyn 2011;1:1–11.

[7] Najjar YSH, Balawneh IAI. Optimization of gas turbines for sustainable turbojet propulsion. Propuls Power Res 2015;4:114–21.

[8] Swe T, Zin WT, Phyo WT. Operational optimization of micro gas turbine engine for higher performance. Development 2018;5.

[9] Turan Ö. Mach number effect on the thermodynamic efficiencies of a turbojet engine: an UAV application. Niğde Ömer Halisdemir Üniversitesi Mühendislik Bilim Derg 2018;7:848–63.

[10] Ahadi Nasab MR, Ehyaei MA. Optimization of turbojet engine cycle with dual-purpose PSO algorithm. Mech Ind 2019;20.

[11] Hendricks ES, Gray JS. pyCycle: A Tool for Efficient Optimization of Gas Turbine Engine Cycles. Aerospace 2019;6. https://doi.org/10.3390/aerospace6080087.

[12] Cent Tai V, Chiak See P, Mares C, Uhlen K. Optimisation of energy and exergy of two-spool turbofan engines using genetic algorithms. ArXiv E-Prints 2012:arXiv-1207.

[13] Bastani M, Jafari R, Ghasemi H. INTERNATIONAL JOURNAL OF ENGINEERING SCIENCES & RESEARCH TECHNOLOGY EXERGY ANALYSIS OF AN AIRCRAFT TURBOJET ENGINE n.d.

[14] Şöhret Y. Ecologic performance and sustainability evaluation of a turbojet engine under on-design conditions. Aviation 2018;22:166–73.

[15] Nikaein M. Multi-objective optimization of gas turbine power cycle. Int J Chem Mol Eng 2011;5:322–7.

[16] Xue R, Jiang J, Jackson A. Effect of bypass ratio on optimal fan outer pressure ratio and performance for turbofan engines. Int J Aeronaut Sp Sci 2019;20:157–64.

[17] Asundi SA, Ali SF. Parametric Study of a Turbofan Engine with an Auxiliary High-Pressure Bypass. Int J Turbomachinery, Propuls Power 2019;4:2.

[18] Jakubowski R. Study of bypass ratio increasing possibility for turbofan engine and turbofan with inter turbine burner. J KONES 2019;26:61–8.

[19] Khalid SJ. Aerothermodynamic benefits of mixed exhaust turbofans. 52nd AIAA/SAE/ASEE Jt. Propuls. Conf., 2016, p. 4641.

[20] Jakubowski R. Analysis of thermodynamic cycle influence of turbofan mixer engine on its performance. J KONES 2009;16:171–8.

[21] Cleary S. The Supersonic Performance of High Bypass Ratio Turbofan Engines with Fixed Conical Spike Inlets 2018.

[22] Kurzke J, Halliwell I, Kurzke J, Halliwell I. New Engine Design. Propuls Power An Explor Gas Turbine Perform Model 2018:3–114.

[23] Marszalek N. Preliminary analysis of thermodynamic cycle of turbofan engine fuelled by hydrogen. J KONES 2018;25:347–54.

[24] Najjar YSH, Al-Sharif SF. Thermodynamic optimization of the turbofan cycle. Aircr Eng Aerosp Technol 2006;78:467–80.

[25] Nordqvist M, Kareliusson J, da Silva ER, Kyprianidis K. Conceptual Design of a Turbofan Engine for a Supersonic Business Jet. Int. Symp. Air Breath. Engines, ISABE 2017, Manchester, United Kingdom, 3-8 Sept. 2017 Pap. no. ISABE-2017-22635, 2017, p. 2580–97.

[26] Zaid I, Ehab M, Mahrous A, El-Sayed A, Emeara M. Performance Analysis of High Bypass Turbofan Engine Trent 1000-A *. 2018.

[27] Ou M, Yan L, Tang J, Huang W, Chen X. Thermodynamic performance analysis of ramjet engine at wide working conditions. Acta Astronaut 2017;132:1–12.

[28] Holst KR. A method for performance analysis of a ramjet engine in a free-jet test facility and analysis of performance uncertainty contributors 2012.

[29] Kraiko AN, Egoryan AD. Comparison of thermodynamic efficiency and thrust characteristics of air-breathing jet engines with subsonic combustion and burning in stationary and nonstationary detonation waves. AIP Conf. Proc., vol. 2027, AIP Publishing; 2018.

[30] Liu Z, Ren X, Yan Z, Zhu H, Zhang T, Zhu W, et al. Effect of inlet air heating on gas turbine efficiency under partial load. Energies 2019;12:3327.

[31] Ibrahim TK, Mohammed MK, Awad OI, Mamat R, Abdolbaqi MK. Thermal and Economic Analysis of Gas Turbine Using Inlet Air Cooling System. MATEC Web Conf., vol. 225, EDP Sciences; 2018, p. 1020.

[32] Arabi S, Ghadamian H, Aminy M, Ozgoli HA, Ahmadi B, Khodsiani M. Energy performance analysis of GE-F5 gas turbines at off-design conditions by applying an innovative convergent–divergent system for the inlet air cooling. Meas Control 2019;52:002029401987750. https://doi.org/10.1177/0020294019877504.

[33] Sabzehali M, Alibeigi M. Comparison of Mixed and Unmixed Turbofan Engine with Intake Air

Cooling: Parametric Study and Optimization-TOPSIS Decision. EasyChair; 2022.